AD-A081 516 EXTRANUCLEAR LABS INC PITTSBURGH PA F/G 11/6
METAL ION REACTIONS WITH OZONE AND ATOMIC OXYGEN.(U)
APR 79 W L FITE, M W SIEGEL, H H LO F19628-77-C-0236
UNCLASSIFIED AFGL-TR-79-0092 NL

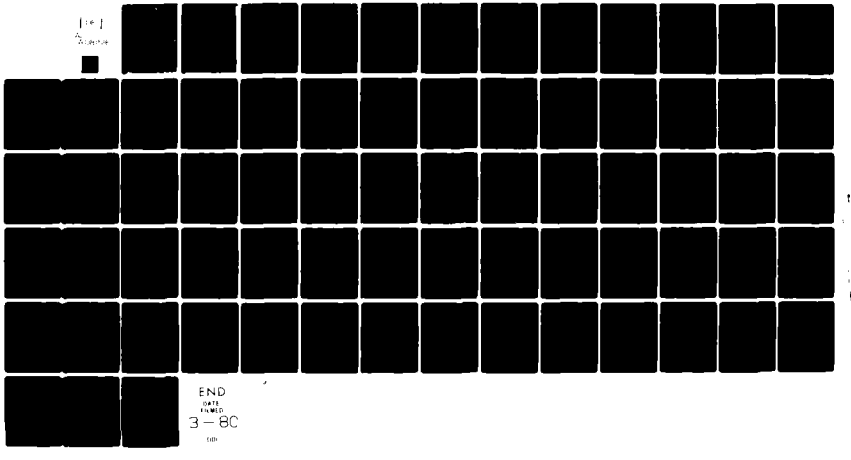

END
DATE FILMED
3-80
DTIC

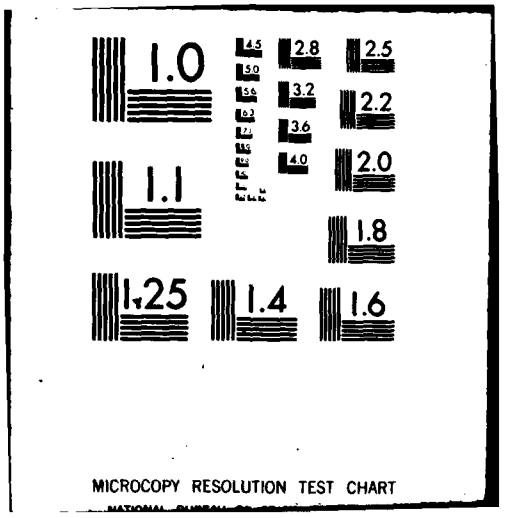
1.0
1.1
1.25
1.4
1.6
1.8
2.0
2.2
2.5
2.8
3.2
3.6
4.0
4.5
5.0
5.6
6.3
7.1
8.0
9.0
10
11
12
14
16
18
20
22
25
28
32
36
40
45
50
56
63
71
80
90
100
MICROCOPY RESOLUTION TEST CHART

[redacted]

# REPORT DOCUMENTATION PAGE

READ INSTRUCTIONS BEFORE COMPLETING FORM

| 1. REPORT NUMBER | 2. GOVT ACCESSION NO. | 3. RECIPIENT'S CATALOG NUMBER |
|---|---|---|
| AFGL-TR-79-0092 | | |

**4. TITLE (and Subtitle)**

METAL ION REACTIONS WITH OZONE AND ATOMIC OXYGEN.

**5. TYPE OF REPORT & PERIOD COVERED**

01 Sep 77 to 31 Dec 78
Final Report

**6. PERFORMING ORG. REPORT NUMBER**

**7. AUTHOR(s)**

W. L. Fite, M. W. Siegel and H. H. Lo

**8. CONTRACT OR GRANT NUMBER(s)**

F19628-77-C-0236

**9. PERFORMING ORGANIZATION NAME AND ADDRESS**

Extranuclear Laboratories, Inc.
250 Alpha Drive
P.O. Box 11512, Pittsburgh, PA 15238

**10. PROGRAM ELEMENT, PROJECT, TASK AREA & WORK UNIT NUMBERS**

62704H, CDNA27 AA
S99QAXHD11, 04

**11. CONTROLLING OFFICE NAME AND ADDRESS**

Air Force Geophysics Laboratory
Hanscom AFB, Maasachusetts 01731
Monitor/K.W.S. Champion/LKB

**12. REPORT DATE**

5 April 1979

**13. NUMBER OF PAGES**

69

**14. MONITORING AGENCY NAME & ADDRESS** *(if different from Controlling Office)*

**15. SECURITY CLASS.** *(of this report)*

Unclassified

**15a. DECLASSIFICATION/DOWNGRADING SCHEDULE**

**16. DISTRIBUTION STATEMENT** *(of this Report)*

Approved for public release; distribution unlimited.

Final rpt. 1 Sep 77 - 31 Dec 78,

**17. DISTRIBUTION STATEMENT** *(of the abstract entered in Block 20, if different from Report)*

**18. SUPPLEMENTARY NOTES**

This research was sponsored by the Defense Nuclear Agency under subtask S99QAXHD411, work unit 04 through Contract F19628-77-C-0236 with the Air Force Geophysics Laboratory.

**19. KEY WORDS** *(Continue on reverse side if necessary and identify by block number)*

Metal ions
Reactions
Ozone
Atomic oxygen
Electron impact ionization

**20. ABSTRACT** *(Continue on reverse side if necessary and identify by block number)*

An experiment attempting to measure the thermal and near-thermal rate coefficients for reactions of metal ions with O and $O_3$ is summarized. The method involves a new type of drift tube made of a fully oxidized leaky dielectric material (Cerramag C-11) which permits placing of the drift field without metallic electrodes which could degrade O and $O_3$ into $O_2$ in surface reactions. In the experiments $Al^+$ from an external surface ionization source was used, the drift gas was argon to which the reactant gas was added, and

DD FORM 1 JAN 73 1473 EDITION OF 1 NOV 65 IS OBSOLETE

38831

SECURITY CLASSIFICATION OF THIS PAGE (When Data Entered)

ions emerging from the drift tube were mass spectrometically detected. It was found by modulated beam mass spectrometry that ozone was not degraded in the drift tube; the atom content in partially dissociated oxygen admitted to the tube was too low to get unequivocal data on the integrity of O in the tube.

The weakness of the available $Al^+$ ion current source limited the amount of Ar that could be admitted to the drift tube before scattering and diffusion reduced the signal of ions emerging from the drift tube to unusably small values. True steady state drift tube conditions could not be achieved. Attempts to measure the mobility of $Al^+$ in Ar were thus not fully successful although the values obtained are not unreasonable. The rate coefficient for formation of $AlO^+$ from $Al^+$ and $O_3$ was not obtainable at thermal and near-thermal energies, although an apparent cross section value of $8 \times 10^{-17}$ $cm^3$ (±33%) was obtained for a narrow energy spread of ions near 9 eV.

The separate measurement of the dissociative ionization cross sections of $O_3$ on electron impact was essential in determining the integrity of the ozone in the drift cell. In this separate measurement, treated in an appendix, the cross sections for formation of $O_3^+$, $O_2^+$ and $O^+$ were measured between threshold and 100 eV in a modulated beam quadrupole mass spectrometer. Phase spectroscopy, which provides a measure of the neutral precursor mass, was used to prove the absence of $O_2$ and O contamination in the ozone beam. Normalized absolute cross sections were measured by calibration against Ar, Ne, and He. Appearance potentials for $O_3 + e \rightarrow O_3^+ + 2e$ (12.67 eV) and $O_3 + e \rightarrow O_2^+ + O \rightarrow 2e$ (13.14 eV) were confirmed, but the observed $O^+$ appearance potential was inconsistent with $O_3 + e \rightarrow O^+ + O_2 + 2e$ (14.7 eV) and probably inconsistent with $O_3 + e \rightarrow O^+ + O + 2e$ (19.81 eV); it was, however, apparently consistent with $O_3 + e \rightarrow O^+ + O^- + O + e$ (18.35 eV).

ESD-3

# METAL ION REACTIONS WITH OZONE AND ATOMIC OXYGEN

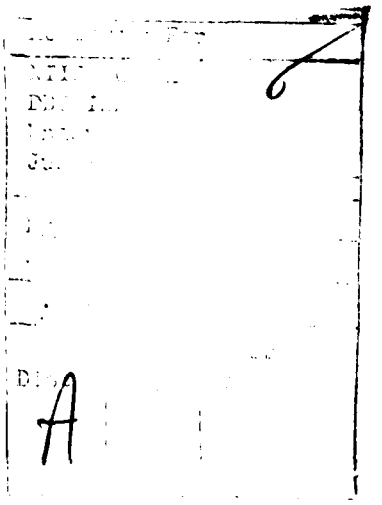

## CONTENTS


| | Page |
|---|---|
| Contents | 3 |
| List of Figures | 4 |
| Introduction | 5 |
| Experimental Approach | 6 |
| Apparatus | 13 |
| Results and Discussion | 21 |
| Conclusions | 28 |
| Acknowledgements | 29 |
| Appendix A | 31 |
| Distribution List | 67 |

## LIST OF FIGURES


| Figure | Caption | Page |
|---|---|---|
| 1 | Schematic of Experiment . . . . . | 8 |
| 2 | Pressure in Drift Tube *vs.* Pressure Measured in Upstream Thermo Gauge . . . . . | 17 |
| 3 | Gating Sequence for Drift Tube Measurements . . . . | 19 |
| 4 | Gating Circuitry . . . . . | 20 |
| 5 | Data for Mobility Measurements of $Al^+$ in Ar, Plotting Et *vs.* E . . . . . | 25 |

## LIST OF FIGURES


| Figure | Caption | Page |
|---|---|---|
| 1 | Schematic of Experiment . . . . . | 8 |
| 2 | Pressure in Drift Tube *vs.* Pressure Measured in Upstream Thermo Gauge . . . . . | 17 |
| 3 | Gating Sequence for Drift Tube Measurements . . . . | 19 |
| 4 | Gating Circuitry . . . . . | 20 |
| 5 | Data for Mobility Measurements of $Al^+$ in Ar, Plotting Et *vs.* E . . . . . | 25 |

# METAL ION REACTIONS WITH OZONE AND ATOMIC OXYGEN

## I. Introduction

In the measurement of thermal-energy charge transfer and ion-molecule reactions of interest in upper atmosphere chemistry, the reactions involving metal ions and atoms have received relatively little attention, and most available rate coefficients are extrapolations downward in energy from ion beam experiments. Thermal energy reactions with metal ions appear to be limited to flowing afterglow measurements by Ferguson and Fehsenfeld[1] for the processes

$$M^+ + O_3 \longrightarrow MO^+ + O_2 \qquad (1)$$

where the metal ion, $M^+$, was $Mg^+$, $Ca^+$ and $Fe^+$, where rate coefficients were measured, and $Na^+$ and $K^+$ where the product ion was not observed, and only an upper limit on the rate coefficient is reported. In reactions of the type

$$M^+ + O + X \longrightarrow MO^+ + X \qquad (2)$$

where X is a third body, no measurements have apparently been made.

Both reactions are of interest for D region chemistry, particularly where the metal ions are $Al^+$ and $Fe^+$.

This report summarizes progress made toward measuring both types of reactions using $Al^+$ and $Fe^+$, using a new drift tube technique.

---

[1] E. E. Ferguson and F. C. Fehsenfeld, J. Geophys. Res. 73, 6215 (1968).

## II. Experimental Approach

In measuring rate coefficients for the reactions of interest, the three requirements are that (1) the gaseous ions of normally solid materials must be made, (2) the chemical integrity of the O and $O_3$ introduced into the experiment must be maintained, and (3) concentrations of the reactant gases must be measurable.

In the approach used here, which is similar to a method first used by Hasted[2] and his collaborators, the ions were produced from a source suitable for making a beam of the ions running through vacuum and then injecting them into a drift tube, where the ions would be rapidly retarded by gas drag to the steady-state drift velocity produced by a uniform electric field in the drift tube. Ions emerging from the drift tube were then mass analyzed and their relative currents measured.

The requirement of the chemical integrity of O and $O_3$ demands an entirely new type of drift tube, however; one which would not cause decomposition of ozone or recombination of O atoms into $O_2$ molecules at interior surfaces of the drift tube. The usual metallic electrodes of drift tubes would not be acceptable.

There exist certain fully oxidized ceramics with electric conductivities in the range of $10^7$ ohm-cm, among which is a cobalt-doped nickel-zinc ferrite produced by Stackpole Carbon Company of St. Marys, Pennsylvania, known as "Cerramag C-11". The resistivity admits producing a uniform electric field inside a hollow tube of the material by applying a potential difference across the ends of the tube, with no interior electrodes. Uniformity of the currents along the length of a hollow cylinder implies a uniform field in the vacuum just inside the cylinder and, therefore, a uniform field in the entire interior volume of the cylinder. The fact that the material is fully oxidized admits the hope that this material would, like glass, not cause the decomposition of ozone and only slowly catalyze the recombination of atomic oxygen.

---

[2] J. B. Hasted, "Measurement of Ion-Molecule Reaction Rates Using Ion Swarms", in "Interactions Between Ions and Molecules", Pierre Ausloos, Ed., NATO Advanced Study Institute Series, Series B: Physics, Volume 6, Plenum Press, New York (1974).

Measurement of the composition of the gas inside the drift tube, by an external means, in order both to verify the chemical integrity of the O and $O_3$ and to obtain the values of the concentrations for determining rate coefficient values, can be done in principle by modulated beam mass spectrometry. However, while the cross sections for electron impact ionization of O and of $O_2$ to produce both $O^+$ and $O_2^+$ are known, it is also necessary to know the fragmentation pattern for production of $O^+$, $O_2^+$ and $O_3^+$ in electron impact ionization of $O_3$. Preliminary knowledge of this fragmentation pattern had already been obtained by M. W. Siegel under Extranuclear Laboratories' in-house research program, but some minor additional studies were appropriate to make in the course of the present experiments.

## A. Basic Experimental Arrangement

The experiment used in the present studies is shown diagrammatically in Figure 1.

The basic instrument used was an EMBA-II modulated beam mass spectrometer, in the second chamber of which are located the modulator wheel, an Extranuclear Laboratories Model 041-1 electron impact ionizer, a Model 324-9 quadrupole mass filter, and an electron multiplier. In some of the measurements the multiplier was a 21-stage Cu-Be unit; for the bulk of the measurements, however, a channeltron multiplier was used because of the necessity of detecting separate ion counts rather than analog ion currents.

The 041-1 ionizer was used in the conventional way when doing the modulated beam mass spectrometry on the gas inside the drift cell. When measuring the ions emerging from the drift cell, the potentials on the ionizer electrodes were changed to make it an einzel-lens to focus the ions into the quadrupole mass filter.

The first vacuum chamber of the apparatus housed the ion source, the drift cell and two planar metal electrodes with apertures immediately before and after the drift cell, that were used as gates in the measurement of the ion mobilities needed in the data analysis, and as focusing lenses in the reaction rate measurements.

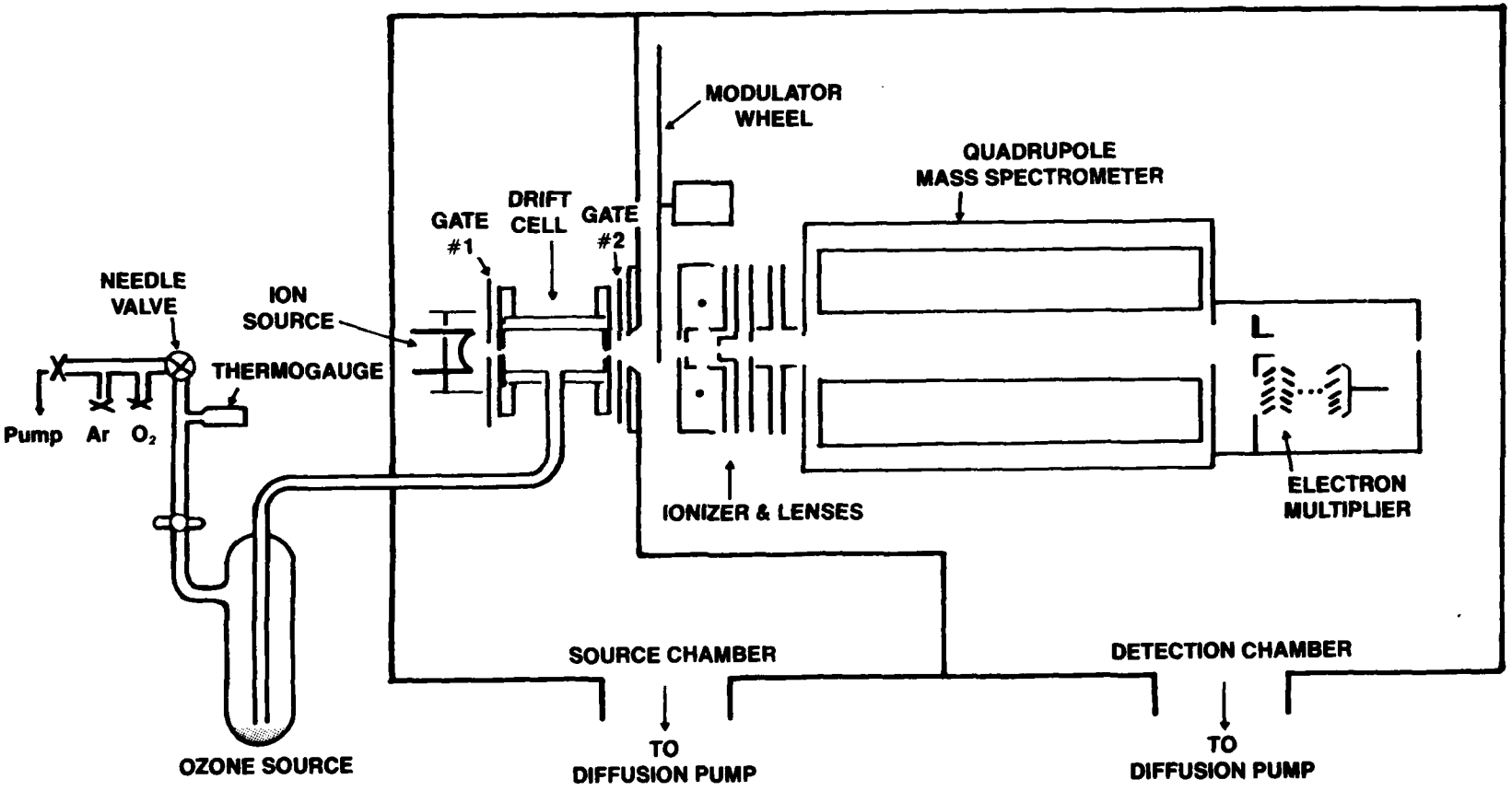


**Figure 1**
**Main Text**

Gas was admitted to the ferrite drift cell through a glass tube from a glass cold trap in which liquid ozone was produced and stored. A teflon stop-cock was interposed between the cold trap and a needle valve, in which a section of line was placed in a thermo-gauge. Tanks of oxygen and argon (the drift gas chosen) were connected, along with a mechanical vacuum pump to a manifold terminated by the needle valve.

Ozone was produced by flowing only oxygen gas through the cold trap and into the drift cell and exciting a radiofrequency discharge by capacitative coupling via external electrodes along the length of larger outside glass of the cold trap. The power source for this discharge was a quadrupole power supply similar to that used to operate the quadrupole mass filter. A liquid nitrogen dewar was raised from below to immerse the lower part of the cold trap in $LN_2$. The discharge was allowed to operate for several minutes until about 0.05 $cm^3$ of solid ozone was frozen onto the walls of the trap. The oxygen flow was then turned off, and Ar flow started. By briefly lowering the $LN_2$ dewar, the ozone was liquified and collected in a droplet at the bottom of the trap. The Ar successfully prevented the ozone from reaching back to the thermocouple gauge and needle valve and carried ozone with it into the drift cell. By exchanging the liquid nitrogen dewar with one containing liquid oxygen, the maximum $O_3$ pressures in the cold trap could be changed from 43 mTorr (at $77^oK$) to 620 mTorr (at $90^oK$). The actual pressure in the drift cell depended on the Ar flow and the amount of liquid or solid ozone surface exposed as well as the choice of liquid gas.

## B. Theory of the Measurement

### 1. Rate Coefficient Determination

When primary ions at an initial concentration $n_o^+$ are placed in an environment containing molecules at a much larger concentration $n_r$ with which the ions can react to form secondary ions, the concentrations of the primary and secondary ions, $n_1^+$ and $n_2^+$, as functions of time are given by

$$n_1^+ = n_o^+ \exp(-n_r k t) \tag{3}$$

and

$$n_2^+ = n_o^+ (1 - \exp(-n_r k t)) \tag{4}$$

where k is the rate constant. The ratio of the secondary to primary ion concentrations is

$$n_2^+/n_1^+ = \exp(n_r kt) - 1 \tag{5}$$

In a drift tube, the drift velocity of the primary ions is given by

$$v_d = KE \tag{6}$$

where K is the mobility of the primary ions in the gas mixture in the drift tube, consisting of a drift gas at concentration $n_d$ plus the reactant gas at concentration $n_r$ and E is the drift field. The time that a primary ion is in the environment, for use in Eqs. (3), (4) and (5) is

$$t = L/v_d = L/KE \tag{7}$$

Combining Eqs. (5) and (7)

$$n_2^+/n_1^+ = \exp(n_r kL/KE) - 1$$

In the case of a drift tube where the ions are injected at a point on the axis, the "beam" diffuses transversely and eqs. (3) and (4) cannot be used in the written form. Equation (5), however, is usable provided that the diffusion is the same for both the primary and secondary ions. This assumption is explicitly made in the present experiments.

The ions in the present experiment are injected with greater velocity than the drift velocity which has two effects: (1) the total time the primary ion spends in the drift tube is less than given by Eq. (7), and (2) if the rate coefficient is dependent on velocity the rate of ion production during the slowing down period will differ from that during the period of steady state drift in the field.

In the present experiments it is assumed that the slowing down time is negligibly small compared to the time spent at drift velocity and that the time given by Eq. (7) is appropriate to the accuracy sought, recognizing that strictly speaking the measurement will provide a lower limit on the rate coefficient if the rate coefficient is velocity-independent. The methods of investigating the latter point are described by Hasted[2], but to first approximation here it is assumed that any change in rate coefficient during the small slowing down time can be neglected.

Finally it is assumed that primary and secondary ion currents, $I_1$ and $I_2$, measured are proportional to the concentrations inside the drift tube at the exit end. With these assumptions the rate coefficient is given by

$$k = (KE/n_r L) \log(1 + (I_2^+/I_1^+)), \tag{8}$$

for two-body processes. For three-body processes k becomes the product of the rate coefficient and the concentration of the drift gas which because of its high concentration to anything else is the third body species.

2. Mobility Measuremtns

The mobility, K, that is required in Eq. (8) is separately determined using a double gating technique. A square-wave pulse of ions is injected into the drift tube by use of Gate #1 and Gate #2 is opened after a variable delay time to pass an identical square wave current pulse. The delay time is varied and the time, $t_m$, at which the current pulse maximum is determined.

The actual time $t_m$ is made up of two components: the time at steady state drift velocity, and the time spent in travel between the external gates and the drift tube and slowing down to the drift velocity. Designating the latter time as $t_o$, which is independent of the electric field applied across the drift tube,

$$t_m = t_o + L'/KE \tag{9}$$

where L' is the length of that portion of the drift tube where the ions travel at the drift velocity. Multiplying Eq. (9) by E, the electric field and rearranging

$$Et_m = L'/K + Et_o \tag{10}$$

By plotting $Et_m$ as a function of E, a straight line should result, the y-axis intercept being the value of L'/k. At sufficiently high drift gas pressures little error is introduced by substituting the overall length of the tube, L, for the quantity L'.

This approach has the merit of clearly indicating when the drift gas pressure is sufficiently high to ensure steady state drifting within the tube.

It is noted that if the pressure is so low that an ion is accelerated to substantially greater than thermal speeds, the average velocity, $\bar{v}$, is given by

$$\bar{v} = (e\lambda/2m)^{1/2}(E)^{1/2} \tag{11}$$

where $\lambda$ is the mean free path. With $t = L'/\bar{v}$

$$Et_m = CE^{1/2} + t_oE \tag{12}$$

where $C = L'(2m/e\lambda)^{1/2}$. A non-linearity appears in the graph of $Et_m$ at insufficient drift gas pressures.

## III. Apparatus

### A. Ion Sources

In experiments involving injection of ions made by an ion source the distribution of excited states of the ions can have very strong influence on the measured rate coefficients. In the present experiments involving $Al^+$ ions, in order to avoid the excited state problem it was elected to use ions produced by thermal ionization at a hot surface. Two types of sources were examined.

#### 1. Direct Deposition Type

In the direct deposition sources an aluminum-containing compound is applied directly to a surface with high work function. Upon heating the surface, $Al^+$ ions are evolved. In the present experiments the compound was aluminum chloride, prepared by dissolving aluminum metal in hydrochloric acid. The solution was then applied to the metal and allowed to dry. The metals experimented with were tungsten and rhenium in both coiled wire and ribbon form. The source found best used was rhenium which is in ribbon form 0.03 mm thick, 0.76 mm wide and 1 cm long. It was heated by a dc current of 3.0 amps at 1.6 volts.

After producing the ions, taking them through the drift tube when evacuated, focusing them through the aperture in the wall separating the vacuum chamber and into the quadrupole mass filter, tuned to $Al^+$ at wide resolution, typical usable maximum ion currents were $1 \times 10^{-12}$ amps. The only other ion of significance, coming from surface ionization of impurities in the rhenium metal, was $K^+$ at a current of about $10^{-14}$ amps.

While this source produced a steady ion currnet for short periods, it suffered from the problem of all direct deposition sources, namely, depletion of the deposited material. Increased ion currents could be produced only at the expense of reducing the time available for experimentation.

This source at a current of $10^{-12}$ amps gave a steady and stable current to within 2% over periods of a half hour typically.

2. Atom Beam Ionization Type

In order to gain longer running time and/or larger currents, a second source involved forming a beam of neutral Al atoms and either ionizing them by impact of 50 ev electrons or directing the atomic beam onto a rhenium ribbon similar to that in the direct deposition type source for surface ionization. In this case the Al metal was placed in a cylindrical boron nitride container from which the beam emerged through an aperture and which was heated by an external tantalum coil operated at 8.5 amps and 12 volts.

It was found that upon electron impact the $Al^+$ currents transmitted through the mass filter were only comparable to those of the direct deposition source. Electron impact was rejected in part because of the production of excited states in this method, but more because of ionization of residual gases in the vacuum, one ion from which is $C_3H_7^+$ at mass 43 which would interfere with measuring $AlO^+$ at the same mass.

Surface ionization of the beam at the rhenium surface was found to produce comparable currents to those from the direct deposition source and, because of the comparatively inexhaustible supply of aluminum atoms, gave stable currents for long periods of time (days). However because of the limited volume available for placement of an atom beam source, an ionizing filament and the drift tube, it was not possible to provide sufficient heat shielding between the atom beam source and the drift tube. Since the drift tube material is actually a semiconductor, heating from the atom beam source caused its resistivity to decrease. Since the drift field is established by a current in the walls of the drift tube, reduced resistance implies higher currents and even more heating of the drift tube, and a potential runaway situation existed.

The source, therefore, that was used throughout most of this work was the direct deposition type.

B. Drift Tube

As noted earlier, the drift tube was unconventional in that it had to maintain the integrity of ozone and atomic oxygen. It was constructed of

Cerramag C/11 which has a resistivity of $10^7$ ohm-cm, as a cylinder 2.54 cm long, 7.9 mm i.d. and 12.7 mm o.d. End pieces of the shape shown in Figure 1 were of diameter larger than the o.d. of the cylinder, and dished in such a way that the end piece fitted over the outside of the cylinder. The dished central regions of the end pieces were ground down to a thickness of about 1 mm and feathered toward the apertures in the center. The apertures were 1.2 mm in diameter. Electrical contact was made between the end pieces and the mating surface on the end plate. Electrical contact to the end pieces from the voltage source were made around the entire outer perimeter of the end pieces to ensure symmetry of the currents in the end pieces and uniformity of the currents in the walls of the cylinder.

Gas was admitted to the drift tube at a point midway along its length by a glass tube that fitted closely into a hole ground into the tube. No sealants were used between the glass and the drift tube.

It may be noted that placing a hole in the side of the drift tube does distort the field inside the drift tube. It can be shown easily, for example, that forcing the current to flow around a hole in a two-dimensional conductor increases the field in the hole to exactly twice the field that would have been there had there been no hole. The distorted current flow around the hole in a cylinder and its effect on the interior field is straightforward (although tedious) to calculate. Qualitatively it may be noted (a) that since the ions that ultimately would be detected travel near the axis of the tube, the distortions would be small compared to the factor of 2 change at the wall, (b) that symmetry about a midplane perpendicular to the axis at the position of the center of the hole must obtain, so that distortions of the component of the field in the direction of the axis would average out, and (c) that any radial drifts of the ions will also average out (i.e., an ion pushed off the axis on one side of the midplane will be returned to the axis on the other side) and radial motion would tend to increase the path length of the ions slightly and thus make the substitution

of L for L' in Eq. (9) a better approximation. For these initial experiments, it was felt premature to treat the field distortion due to the gas inlet hole in complete detail and it was assumed that the field in the drift tube was uniform.

C. Pressure Measurement

The gas pressure in the drift tube is monitored by the thermo-gauge (Granville-Phillips) shown in Figure 1. This gauge was located 154 cm from the drift tube. Calibration of this monitoring gauge was made by replacement of the drift tube by an identical dummy drift tube into which a second hole had been ground so that an identical thermogauge could be run directly to the drift tube through about 20 cm of 4 mm i.d. glass tubing. Figure 2 shows the calibration plot comparing the drift tube pressure as a function of the up-stream pressure measured by the monitoring gauge for Argon, which was the drift gas used throughout the experiment. The pressures actually used in the experiment were well into the region where the two gauges track linearly.

A second check on pressure in the drift tube was made by noting the pressure change in the first vacuum chamber upon admission of gas to the drift cell and estimating the pumping speed of this chamber's pump (250 liters/sec) to get the total gas flow into the vacuum, and then calculating the pressure inside the drift tube that would produce this gas flow. Agreement was found with the primary calibration measurement described above to 10% or less for Ar, $N_2$, $O_2$ and $O_3$.

D. Ion Gating

For the mobility measurements, square-wave ion current pulses were made using the gates shown in Figure 1. The gates themselves were flat plates with apertures of 3.2 mm. When Gate #1 was opened, its potential was equal to the ion source potential; when closed its potential was increased by 4 volts. The source potential is defined for this purpose as the potential at the negative end of the rhenium ribbon, which was normally about 8 volts above ground. When Gate #2 was open, it was at ground potential; when closed its potential was raised by 12 volts. The distance between the gates

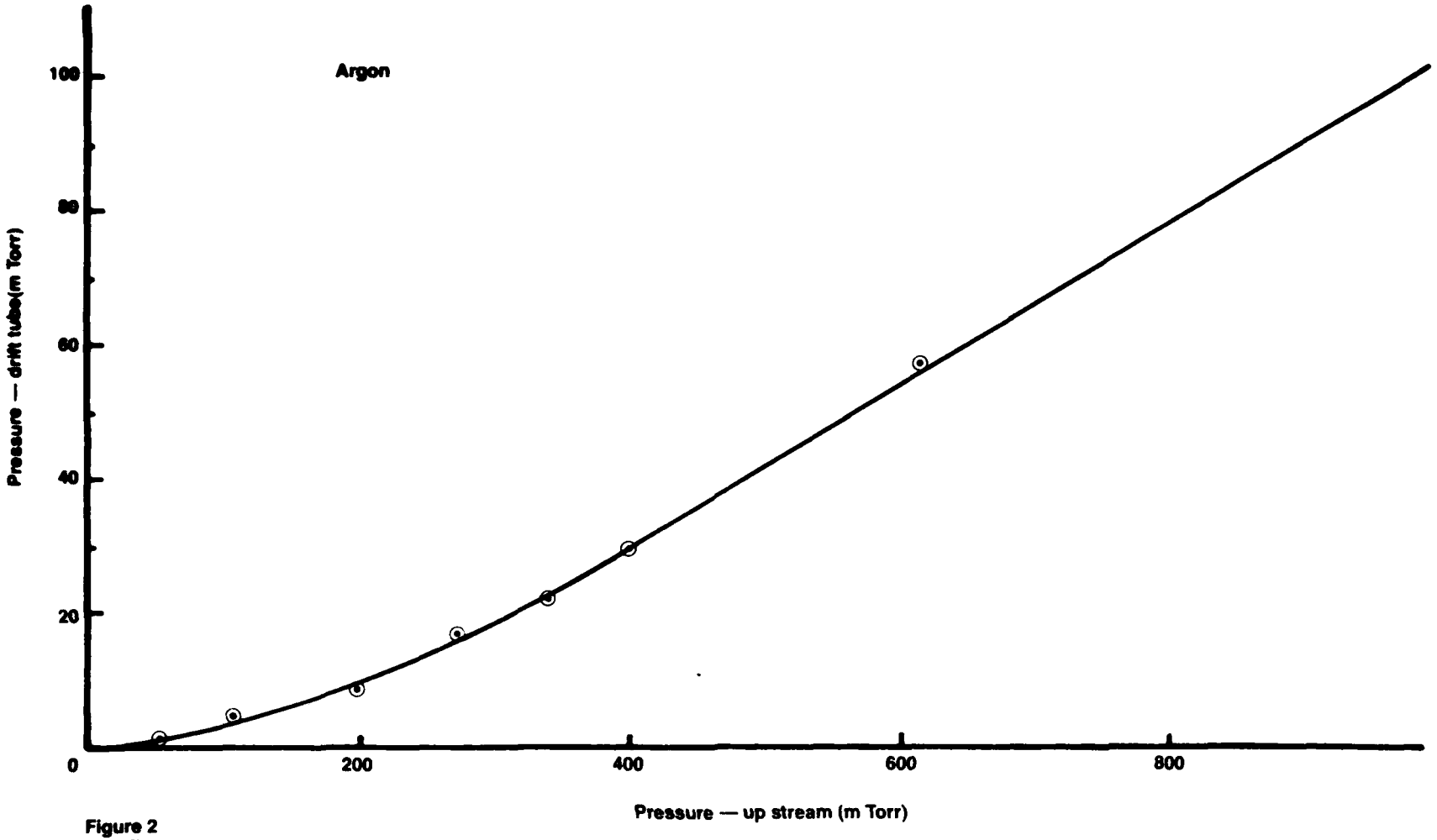


**Figure 2**
**Main Text**

was 3.2 cm so that the space between the gates and the adjacent drift tube ends totalled about 3.5 mm. The entrance aperture of the drift tube was held at the source potential (so that the actual energy of the ions entering the drift cell was determined by the voltage at the center of the rhenium ribbon, about 0.8 volts, neglecting contact potentials). The exit of the drift tube was at a potential of the drift field times the length of the drift tube.

The procedure used in the gating is shown in Figure 3. Gate #1 was opened for a period of 50 microseconds and then closed for a period of 220 microseconds. Gate #2 was operated identically except for a delay time which was variable. The transit time was taken to that delay time corresponding to the maximum ion current being transmitted through the Gate #2.

The gating circuitry is shown in Figure 4.

## E. Ion Detection

The quadrupole mass filter was an Extranuclear Model 4-324-9 and the ionizer was Model 041-1. A 21-stage venetian blind Cu-Be multiplier was used in the current measuring mode when measurements of gas integrity were made. In the reaction and mobility experiments, the very low signal levels required its being used in the ion counting mode.

## F. Ozone Source

The ozone source is described in Appendix A, which is a draft of a paper by M. W. Siegel on the electron impact ionization of ozone. For study of atomic oxygen integrity the same source was used, except that the trap was run at room temperature.

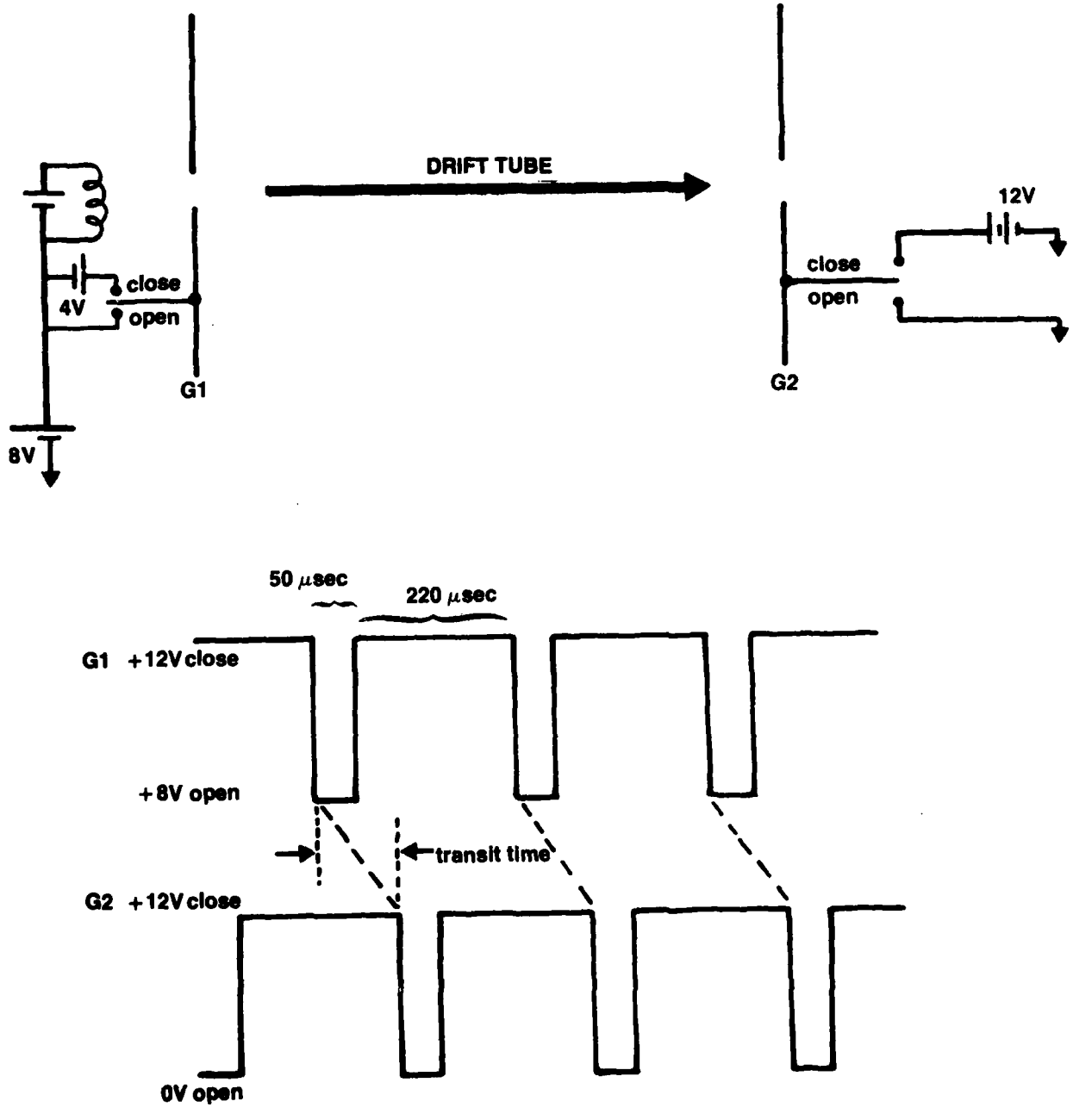


**Figure 3**
**Main Text**

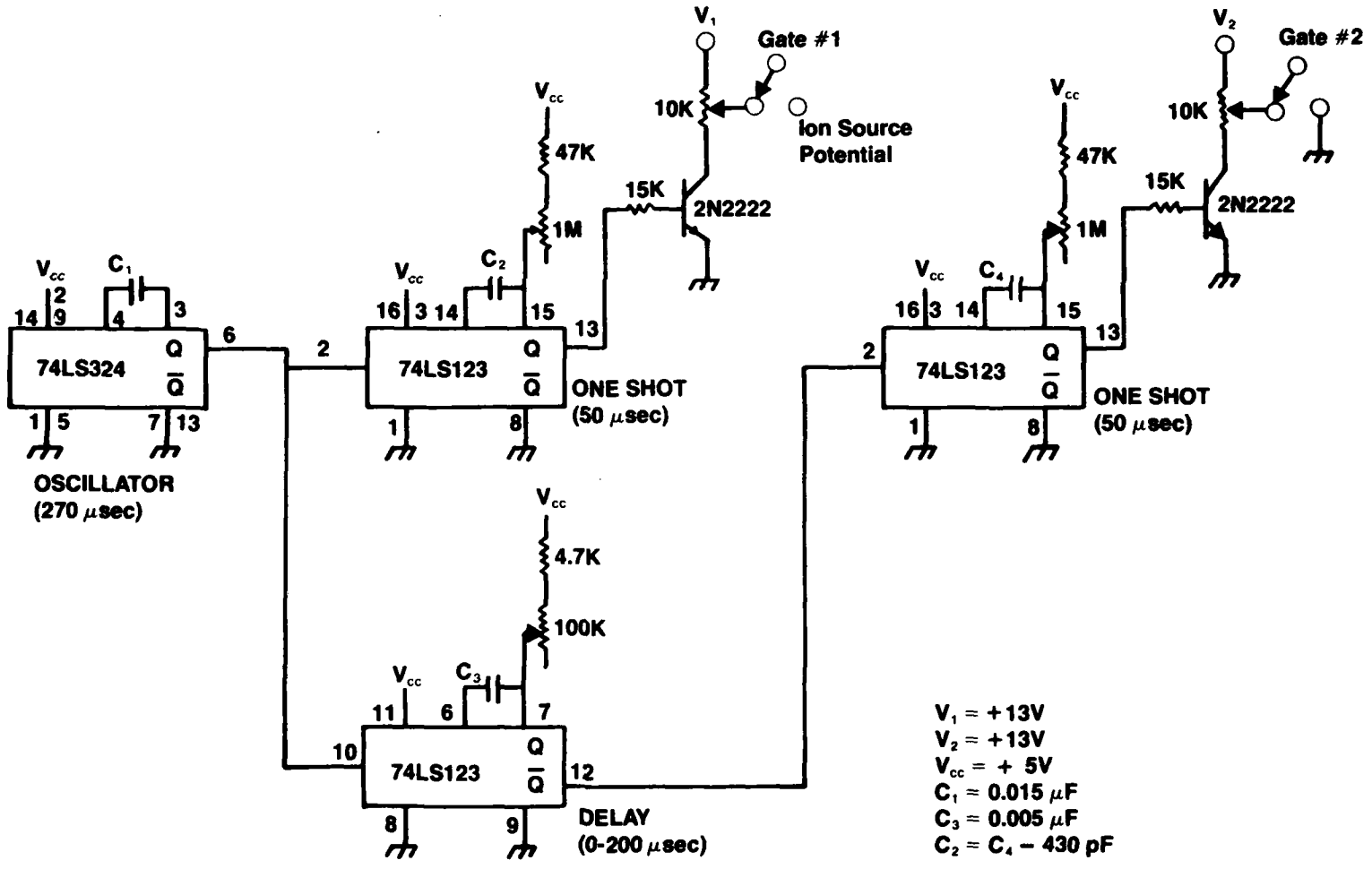


**Figure 4**
**Main Text**

## IV. Results and Discussion

### A. Integrity of Ozone and Atomic Oxygen

The major reason for approaching the measurements of the reactions of interest as was done here was to have a swarm experiment in a tube which would not destroy ozone and atomic oxygen at its interior surfaces. The first problem, therefore, was to determine whether these gases would remain in the drift tube and not be converted by wall reactions back into $O_2$.

Modulated beam mass spectrometry is capable of analyzing all three species. However, the $O^+$ ion at 16 amu is produced not only by ionization of O, but also by dissociative ionization of $O_2$ and $O_3$; the $O_2^+$ ion at 32 amu is produced by dissociative ionization of $O_3$ as well as simple ionization of $O_2$. To measure the gases in the cell it is necessary to know the cracking patterns of the molecules. The cracking pattern of $O_2$, i.e., the ratio of measured $O^+$ and $O_2^+$ currents, is readily measurable by putting pure $O_2$ into a molecular beam source.

Determining the cracking pattern of $O_3$ is not easy, because one must have the assurance that $O_3$ in a molecular beam source is not contaminated by $O_2$ formed from decomposition of the $O_3$.

This problem can be addressed very effectively by using phase spectrometry as well as mass spectrometry in a modulated beam experiment. Appendix A describes experiments of one of us (M. W. Siegel) on this problem. Briefly summarized here, this experiment consisted of producing ozone by discharging oxygen and cryogenically collecting ozone produced, and then feeding the vapor above the liquid ozone via an all-glass line into a glass beam source. By examining the phase of the modulated beam signals of the ions at 16, 32, and 48 amu, it was possible to determine that the ozone was free of $O_2$ contamination in the all-glass system and the ratios of currents of the three ions as a function of electron energy up to the 100 ev maximum energy included in the experiment were measured. Using a standard gas mixture of He, Ne, Ar, and the known ionization cross sections for these gases, the transmission of the mass filter and overall detection efficiency as a

function of mass was determined, from which the relative cross sections for $O^+$, $O_2^+$ and $O_3^+$ production from $O_3$ were determined and, to less reliability, the absolute cross sections as well. (The bulk of this work was done under Extranuclear's in-house research program, but some final points were checked in the course of the present contract).

From Siegel's work it was clear that a test for purity of $O_3$ in the Cerramag drift tube could consist of measurement of the ratio of $O_2^+/O_3^+$ ion currents, after determining the transmission and overall detection efficiency (mass discrimination) using the $Ar^{++}/Ar^+$ ion current ratio, and the known cross sections for the single and double ionization of Ar.

It was found that the $O_2^+/O_3^+$ ratio at 70 ev was 0.66 as compared with Siegel's 0.71 and at 100 ev the ratio was 0.73 as compared to Siegel's 0.74.

The conclusion is that the drift tube maintained the ozone as well as the glass system did, and that the ozone was not being degraded by the tube material.

With regard to atomic oxygen the situation is not clear. It is known that some radio-frequency gas discharge sources of atomic oxygen for atomic beams can produce 20-40% dissociation[3], but the gas is taken directly from the plasma in such sources and the modulated beam mass spectra reveal no significant amount of ozone or any other species in the beam. In other experiments where discharged oxygen has been detected by electron spin resonance after passage along some distance of glass tubing, the dissociation fraction has been found to be typically only of the order of 1%.[4] Since conditions in the drift tube and a few more centimeters of glass tubing leading to the drift tube, the task becomes one of detecting by modulated beam mass spectrometry 1% of oxygen atoms in a beam containing $O_2$ and $O_3$ formed at walls in three-body collisions in the gas, the latter two of which produce $O^+$.

---

[3] W. L. Fite and R. T. Brackmann, Phys. Rev. 113, 815 (1959).

[4] J. W. Linnett, private communication (1960).
H. Wise, private communication (1960).

Experiments were performed on the gas issuing from the drift tube when oxygen flowed in and when the cold trap was not cooled. It was found that the $O^+$ signal increased by about 2% when the discharge power was turned on. However, the experimental uncertainty in the fraction of $O^+$ that is produced by dissociative ionization of $O_3$ and the possibility of excited states of $O_2$ that might not be quenched and which might have an increased dissociative ionization cross section, prevents our drawing any conclusions with respect to the extent to which atomic oxygen remains atomic in the drift tube.

The experiments carried out were not extensive in view of our major attention being directed toward the reactions with ozone.

B. Mobility Measurements

With reference to Section II.B.2, above, a plot of Et vs. E, is shown in Figure 5, for the case of $Al^+$ ions in argon at various pressures in the drift tube.

Particularly to be noted is that at the lower pressures the curves show a decidedly non-linear shape indicating that the pressure in the drift tube is not sufficiently high to cause the ions to get into a steady-state drift at a velocity low compared to the thermal velocity of the Ar.

At the higher pressure shown (78 mTorr) the curves for two typical runs are apparently linear up to a drift field of about 1 V/cm, but then turn downward. Ignoring the higher E points and extrapolating to the vertical axis intercepts (37 and 44 V-μsec/cm), and using Eq. (10), mobilities of $6.8 \times 10^4$ and $5.7 \times 10^4$ $cm^2$/V-sec at a pressure of 78 mTorr and a temperature of $323^oK$, are inferred. Using the formula

$$K_o = K \frac{P}{760} \frac{273}{T,}$$

the average zero-field mobility at $0^oC$ and atmospheric pressure is calculated to be 5.45 $cm^2$/V-cm.

This number is almost certainly wrong. First, at the 78 mTorr pressure, the mean free path is not negligibly small compared to the length of the drift

tube; it is doubtful that the ions are being slowed from their injection velocity down to a steady state drift velocity and that substituting L for L' is appropriate. Second, according to the classical Langevin theory, which predicts values in good agreement with experiments on alkali ions in Ar, Kr, Xe, $N_2$ and $H_2$[5], gives a calculated value of 2.69 $cm^2$/V-cm, about half the "measured" value, for the zero-field STP mobility.

The problem is, of course, that the pressure in the drift tube could not be raised sufficiently high to ensure steady state drift without intolerable attentuation of detectable signal through scattering and transverse diffusion of the beam as it proceeded through the drift tube. It is to be recalled that the maximum primary ion currents used were of the order of $10^{-12}$ amps and this is four to six orders of magnitude less than the primary currents used in other experiments where ion injection of ions into a drift tube had been successful.[2]

Admitting the failure to achieve steady state drift, an attempt was made to obtain a *believable mobility value* by obtaining a correction factor to the measured value. This attempt involved measuring the mobility by the method used here for $K^+$ in Ar, and then comparing it with the known values determined in other drift tube experiments.[5]

In this experiment, a surface ionization source of $K^+$ was used and measurements were made at a pressure of 42 mTorr in the drift tube at a temperature of $323^oK$. The vertical axis intercept was obtained by extrapolating the lowest two points linearly to E = 0. The zero-field mobility value, for $0^oC$ and atmospheric pressure, was given as 10.7 $cm^2$/V-sec, which is a factor of 4.1 times the accepted value of 2.64 $cm^2$/V-sec.

Using the 54 m-Torr data of Figure 5, the same procedure yields a value of 16.8 $cm^2$/V-sec. When divided by 4.1, the value of 4.1 $cm^2$/V-sec is obtained, which is probably still too high.

---

[5]A. M. Tyndall "The Mobility of Positive Ions in Gases", Cambridge University Press, Cambridge, England, 1938.

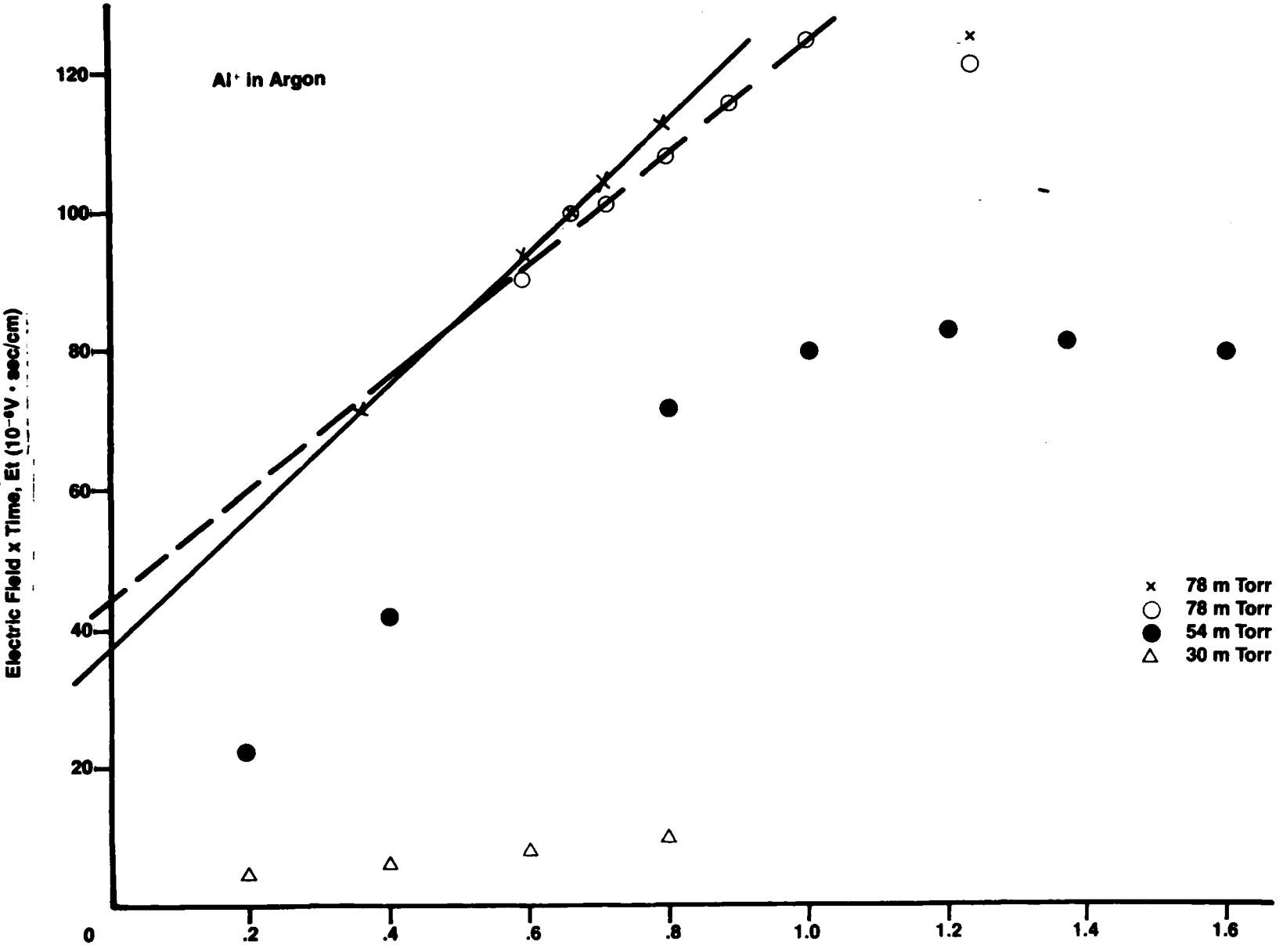


Figure 5
Main Text

As a matter of completeness, it was found that attenuation of the $Al^+$ beam by Ar in the drift tube used in these experiments caused an attenuation by a factor of about 10 for every 20 mTorr of pressure in the drift tube.

C. $Al^+ + O_3$ Reaction

Very early in the program the reaction $Al^+ + O_3 \rightarrow AlO^+ + O_2$ was observed. In this first observation, ozone alone was admitted to the drift cell. It was found that the $Al^+$ beam was attenuated by almost exactly a factor of 10 and the ratio of $AlO^+/Al^+$ was 0.02 when the ozone reservoir was held at liquid oxygen temperature. The ion energy was approximately 8.1 ev upon entering the drift tube and the field inside the drift tube was 0.8 V/cm.

In view of our not being able to complete the full measurements in the drift gas as originally planned, it is worthwhile examining this first observation in light of what was subsequently determined.

First, we believe that the ozone was in fact pure, high quality ozone in view of the experiments described in Section IV.A, above. Second, the pressure in the drift tube, estimated from the pressure rise in the first vacuum chamber and the pumping speed was 0.002 Torr; the pressure in the drift tube deduced from the curve in Figure 2 and the measured pressure at the thermo gauge near the entrance to the cold trap, was 0.004 Torr. In view of the uncertainties of similarity of ozone to argon for thermo gauge response and the non-linearity in the relevant low pressure region of Figure 2, the latter figure is not considered reliable, and in view of chemical changes of the ozone at surfaces (possibly oil coated) in the first chamber the former figure can also not be trusted. For present purposes we take the pressure in the drift tube as 0.003 Torr (±0.001 Torr).

Taking the number density of ozone in the drift cell as $9.6 \times 10^{14}$ $cm^{-3}$, the factor of 10 attenuation of the $Al^+$ beam over the cell length of 2.5 cm indicates that the total $Al^+$ loss cross section (scattering plus reaction) is $9.5 \times 10^{-15}$ $cm^2$ (±33%) at an average ion energy of 9.1 ev.

Because of the high energy, Eq. (5) for a rate coefficient seems less appropriate to use than a cross section formula. Defining $Q_r$ as the cross section for reaction, the ratio, R, of $AlO^+/Al^+$ is given by

$$R = n\, Q_r\, L \tag{12}$$

in the limit of small values of R. For R = 0.02, and with n and L as taken above, $Q_r$ is calculated to be $8.2 \times 10^{-17}$ $cm^2$.

Because the relative velocity distribution is sharply peaked at the $Al^+$ velocity, a rate coefficient determination consists only of multiplying $Q_r$ by the $Al^+$ velocity, $8.2 \times 10^5$ cm/sec, yielding $k = vQ_r = 6.4 \times 10^{-11}$ $cm^3$/sec. It is emphasized that this is a super-thermal rate coefficient, at an energy of 9.1 ev and is subject to uncertainties of an estimated 33%.

## V. Conclusions

The principal conclusions of this work are:

1. The use of leaky dielectrics as drift tubes is a viable alternative to using drift tubes in which metallic electrodes are placed to produce the drift field.

2. Cerramag C/11 is a good material to use for the drift tube, in the sense that ozone is not degraded in wall reactions. Whether it is a good material for maintenance of atomic oxygen in the drift tube was not definitively determined.

3. It was found that to perform drift experiments on $Al^+$, using the ion injection approach pressures of Ar drift gas of 78 mTorr and less are inadequate to establish steady state drift conditions. It appears that a pressure of at least 200 mTorr would be required in the drift tube and from the measured attentuation of the $Al^+$ beam in Ar a primary ion source current of the order of $10^{-6}$ amps would be necessary in order to have output signals in the 100 counts/second range. These magnitudes of currents are not producible with direct deposition sources of the type used here, if they are to operate for a period long enough to make the measurements.

4. If this approach for experiments with $Al^+$ is used again, the type of ion source which should be investigated is that in which a metallic aluminum beam is directed toward a hot rhenium surface where the aluminum atoms are surface ionized. Ample space should be provided to permit the use of sufficient heat shielding between the atom beam source and the drift tube, if the drift tube is a semiconductor such as Cerramag C/11 is.

## VI. Acknowledgements

We wish to acknowledge helpful conversations in the course of this work with Mr. R. T. Brackmann and Dr. T. A. Patterson.

APPENDIX A

# Cross Sections for Production of $O_3^+$, $O_2^+$, and $O^+$ by Electron Impact Ionization of Ozone Between Threshold and 100 eV

M.W. Siegel
Extranuclear Laboratories, Inc.
P.O. Box 11512
Pittsburgh, PA 15238

CONTENTS


| | Page |
|---|---|
| Contents | 33 |
| Figures | 34 |
| Abstract | 35 |
| Introduction | 37 |
| Apparatus | 37 |
| Method and Calibration | 42 |
| Modulated Beam Mass Spectrometry and Phase Spectrometry | 43 |
| Near Threshold Data | 48 |
| Broad Range (Threshold to 100 eV) Data | 53 |
| Appendix | 61 |

## FIGURES


| Figure | | Page |
|---|---|---|
| 1 | Ozone Source . . . . . | 38 |
| 2 | Vacuum Chamber . . . . . | 40 |
| 3 | Data Layout . . . . . | 41 |
| 4 | $\Delta f/\Delta \ell$ . . . . . | 47 |
| 5 | Near Threshold Data - Lin . . . . . | 49 |
| 6 | Near Threshold Data - Log . . . . . | 50 |
| 7 | Energy Levels . . . . . | 52 |
| 8 | Deviation, our Ar, Ne, He to Ks . . . . . | 55 |
| 9 | Trans. vs El. Energy . . . . . | 57 |
| 10 | Data & Kieffer . . . . . | 60 |

## ABSTRACT

Cross sections for the electron impact ionization of ozone to $O_3^+$, $O_2^+$, and $O^+$ are measured between threshold and 100 eV in a modulated beam quadrupole mass spectrometer. Phase spectroscopy, which provides a measure of the neutral precursor mass, is used to prove the absence of $O_2$ and O contamination in the ozone beam. Normalized absolute cross sections are measured by calibration against Ar, Ne, and He. Appearance potentials for $O_3 + e \rightarrow O_3^+ + 2e$ (12.67 eV) and $O_3 + e \rightarrow O_2^+ + O \rightarrow 2e$ (13.14 eV) are confirmed, but the observed $O^+$ appearance potential is inconsistent with $O_3 + e \rightarrow O^+ + O_2 + 2e$ (14.7 eV) and probably inconsistent with $O_3 + e \rightarrow O^+ + O + O + 2e$ (19.81 eV); it is, however, apparently consistant with $O_3 + e \rightarrow O^+ + O^- + O + e$ (18.35 eV).

## INTRODUCTION

The ionization potential of ozone is known from photoionization measurements (12.67 ev), but its electron impact ionization cross sections, appearance potentials, and fragmentation channels have apparently not previously been reported. We were prompted to make these measurements by our need to know the electron impact ionization cross sections for calibration of the ozone beam intensity in separate experiments on associative ionization between actinide metals and ozone. We expect the results reported here will be useful in atmospheric and environmental studies, and also as an example of the application of phase spectrometry to the identification of the neutral precursors of observed mass spectrometric ions.

### Apparatus

Ozone was produced by a RF discharge in flowing oxygen at several torr, and frozen onto the walls of the all-glass source (Figure 1) by a liquid nitrogen bath (mp $O_3$ = -192.7°C; bp $N_2$ = -195.4°C). After about 10 minutes the discharge was turned off and the $LN_2$ dewar slowly lowered, the liquid ozone forming an approximately 0.1 $cm^3$ puddle in the bottom of the source vessel. The $LN_2$ was then quickly replaced by a liquid oxygen bath, at which temperature (bp $O_2$ = -183.0°C) the ozone vapor pressure was sufficient to generate an adequate beam which remained stable for many hours.

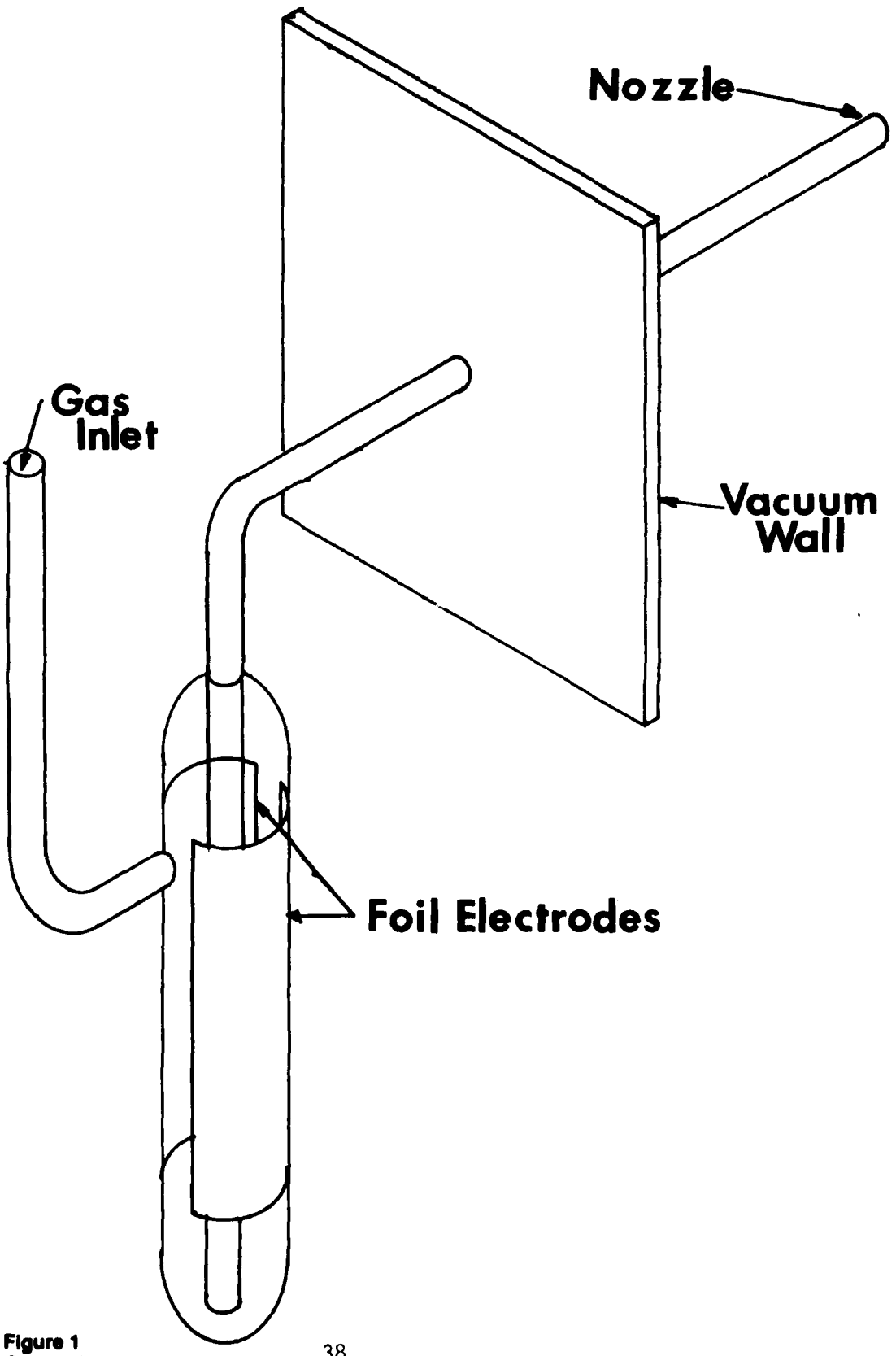


Figure 1
Appendix

The ozone beam was formed by a glass nozzle, an integral part of the source, with an aperture approximately 1 mm in diameter removed approximately 1 cm from an approximately 1 mm differential pumping aperture in the wall dividing the two-chamber vacuum system (Figure 2). A toothed wheel modulator chopped the beam enroute to the ionizer, and a light source-phototransistor pair provided the reference signal for a phase sensitive ("lock-in") amplifier observing the output of a conventional electrometer preamplifier.

The beam was ionized by electron bombardment, and the ions mass filtered and detected by a quadrupole mass spectrometer equipped with a Cu-Be dynode multiplier. This apparatus, excluding the ozone source, is an Exttanuclear Laboratories, EMBA-II modulated beam mass spectrometer system, with turbo-molecular pumping and continuously variable modulator-to-ionizer distance options. A minor temporary modification to the ionizer control allowed the electron energy to be swept by an external ramp generator. A logarithmic amplifier inserted between the lock-in amplifier output and chart recorder input was used to record broad energy range (10-100 ev) cross section data. For increased precision near ion appearance thresholds, narrow energy range scans (10-30 ev) were recorded linearly and where appropriate numerically reduced to semi-logarithmic plots later. A second pen on the chart recorder was used to record the instantaneous electron energy, thereby obviating any need to rely on sweep speed and linearity or scanning range reproducibility to obtain electron energy calibration and correspondence. The apparatus and data systems are shown in block diagram form in Figure 3.

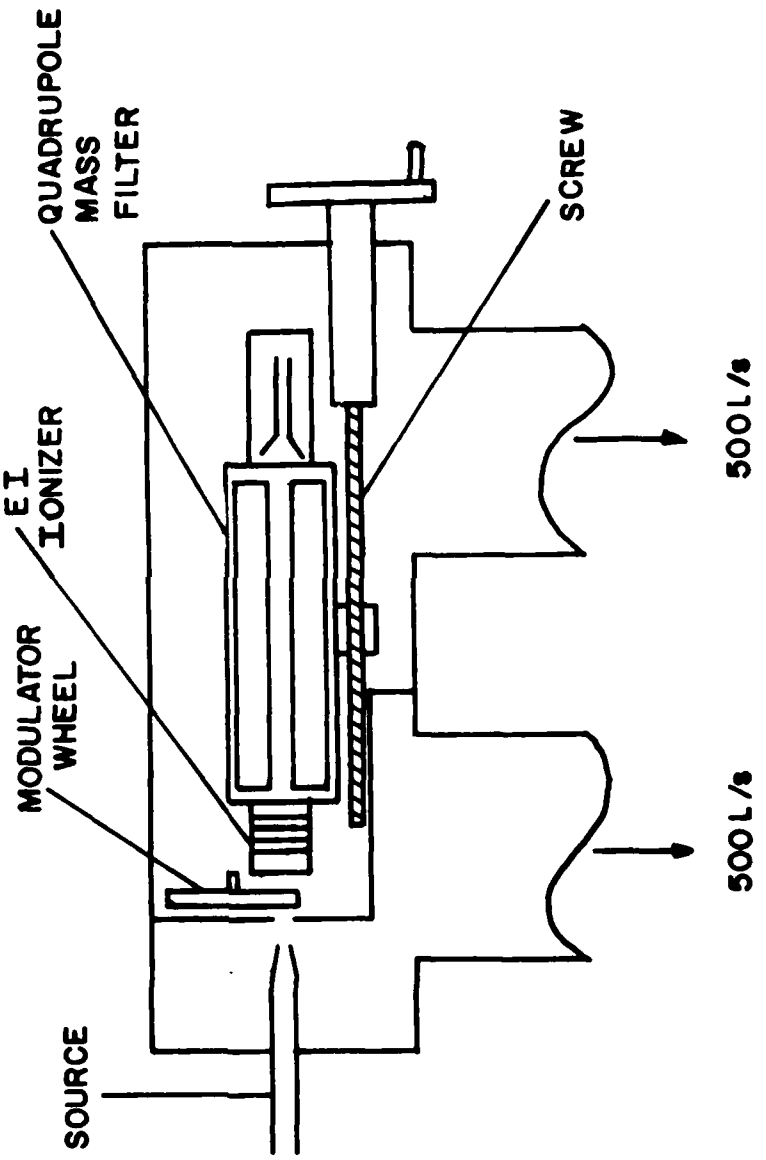


Figure 2
Appendix

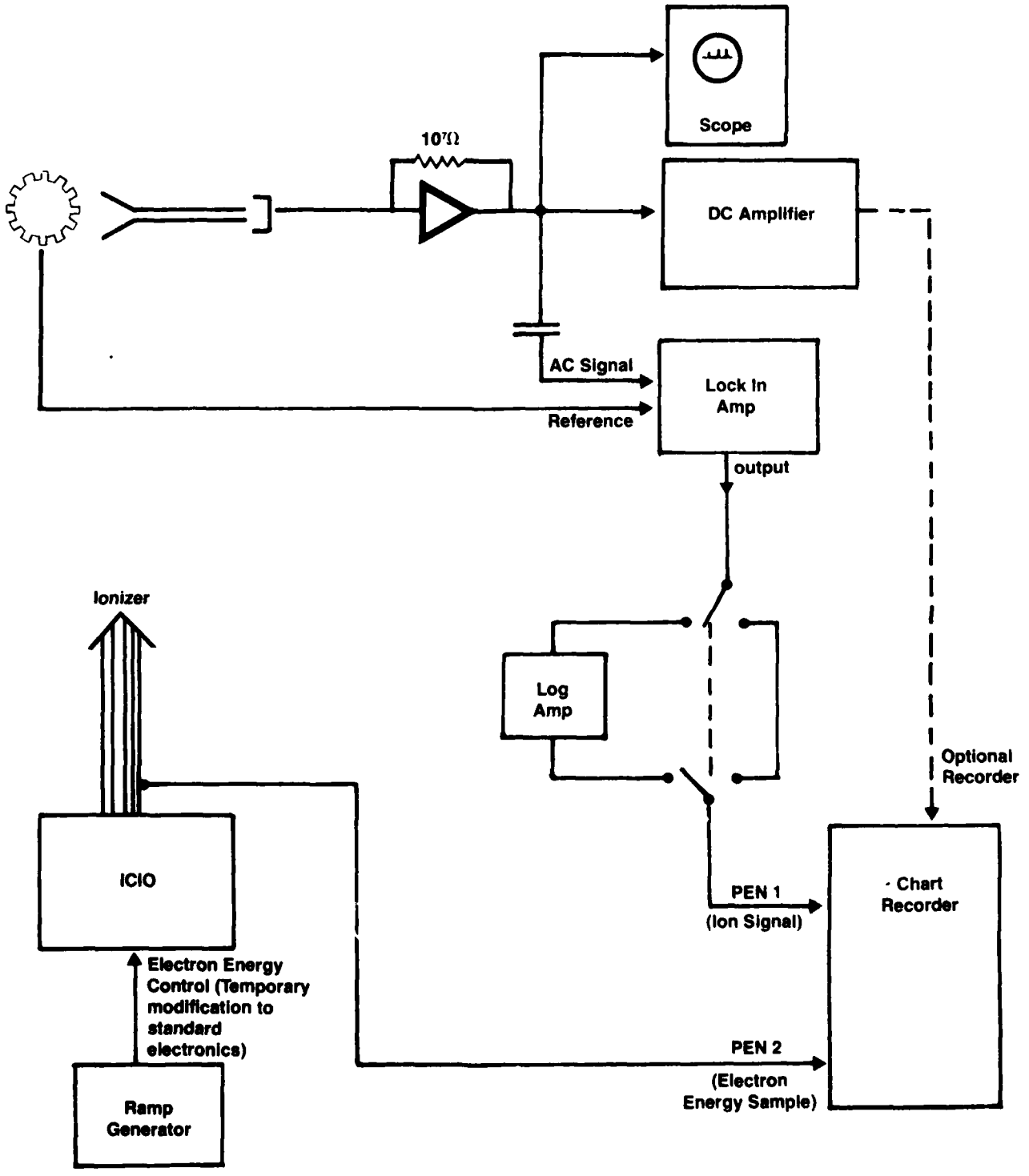


**Figure 3**
**Appendix**

Method and Calibration

To provide calibration for the absolute cross section determination, and also to provide the information needed to determine the ion mass dependence and the electron energy dependence of the instrument sensitivity (ion current/electron emission-pressure-cross section), a mixture of He, Ne, and Ar was prepared by macroscopic partial pressure addition . Measured electron impact cross sections for total ionization of these gases have been critically evaluated and tabulated, and we can take them as benchmarks suitable for instrument calibration. These reference data are henceforth collectively referred to as Kieffer's, after the name of the compiler. While Kieffer's data are for total ionization, and our measurements are for single ionization, valid comparison is nevertheless easily accomplished. In the energy range of interest at our cross section resolution, the cross sections for production of $He^{++}$ and $Ne^{++}$ are negligible. The cross section for production of $Ar^{++}$ is significant above about 55 ev, but this ion can be observed at m/e = 20 and added* to the observed $Ar^{+}$ current for comparison with Kieffer's data. The presence of $^{40}Ar^{++}$ superimposed on $^{20}Ne^{+}$ is no problem because Ne can be observed as $^{22}Ne^{+}$.

The rare gas mixture was used as a buffer-carrier gas at a pressure approximately 10 times the $O_3$ pressure at liquid oxygen temperature. The accuracy of this relative pressure measurement is obviously a critical point in obtaining absolute cross sections, and in fact is the

*Simple addition is actually appropriate only when detection is by a Faraday cup. When a particle multiplier is used, twice the $Ar^{++}$ signal should be added to the $Ar^{+}$ signal, since the multiplier responds more nearly to the number of ions incident per second than to the total charge incident per second. Kieffer's total ionization data are just that: $Ar^{++}$ ions contribute twice as much to the total as $Ar^{+}$ ions do.

limiting factor in determining the absolute accuracy of our reported results. Circumstances beyond our control* made a very good pressure measurement impossible, although it is perhaps doubtful that any general purpose pressure measuring device can give a reliable measurement for ozone. A capacitance manometer, for example, might give questionable results because of ozone decomposition on the metal diaphragm. Our approach, admittedly expedient, was to use a thermocouple gauge communicating with the source volume through a fairly low conductance unswept path; our assumption is that there was little or no ozone in the gauge tube, but the pressure in the gauge tube was the same as the pressure in the source.

In order to observe the effect of replacing the $O_3$ with $O_2$, part of the rare gas mixture was bled off and further mixed with $O_2$ at a concentration approximating the $O_3$ concentration during normal operation. Thus normal operation consisted of observing $He^+$, $Ne^+$, $Ar^+$, $O_3^+$, $O_2^+$, and $O^+$ from ozone at liquid oxygen temperature, with the rare gas buffer present, and checking operation consisted of observing $He^+$, $Ne^+$, $Ar^+$, $O_2^+$, and $O^+$ from ozone at liquid nitrogen temperature, with the rare gas and oxygen mix present. Tanks of the rare gas mix and rare gas plus oxygen mix have been preserved for future reference.

Modulated Beam Mass Spectrometry and Phase Spectrometry

When the ozone-containing beam is modulated, the $O_3^+$, $O_2^+$ and $O^+$ ion signals due to ozone molecules in the beam retain the modulation.

*The instrument was available only during the period between its assembly and its shipment to Extranuclear's customer; these experiments were conducted as part of the quality control tests.

An AC signal amplifier tuned to the modulation frequency sees only the ion signal due to beam components, and is blind to the DC ion signals due to background molecules. Of special interest is that the AC channel is blind to specific background molecules such as $O_2$, $NO_2$, $H_2O$ which contribute to the total (AC + DC) signals at me = 32 and 16. Thus beam modulation and AC detection provide a powerful means of simplifying mass spectra by automatically subtracting out the background. Significant enchancement in usable sensitivity accompanies this simplification in spectra, but this enhancement is only marginally relevant in the present measurements.

When the AC signal amplifier is of the phase sensitive ("lock-in") type, an even more powerful technique becomes available; the ability to do time-of-flight mass spectrometry on the neutral precurser of any ion mass signal, and thus to identify the molecular weight of the neutral species from which each ion mass spectral peak is derived. By this additional technique ("phase spectrometry") we demonstrate that the $O_3$ beam is free of contaminants (such as $O_2$, CO, $H_2O$, etc.) which might contribute to the total AC signal at m/e 32 and 16. The major concern, of course, is that the "ozone" beam might contain a significant $O_2$ contaminant. If this were the case and we were ignorant of it, the cross sections measured for the production of $O_2^+$ and $O^+$ from $O_3$ would be irretrievably in error.

To review the technique of phase spectrometry, first consider the simplified case of a monoenergetic beam, all of whose molecules travel at the same velocity v. If this beam is modulated at frequency f, then in an ionizer downstream by distance $\ell$ an ion signal will be developed with a phase

with respect to the phase at the modulator. It is easily derived that for this monoenergetic beam

$$\frac{\phi}{360^o} = \frac{f\ell}{v}$$

where $\phi$ is in degrees.

In a beam with a distribution of molecular velocities, the mean phase shift $\phi$ is determined by integration of this result over the velocity distribution. For the case of a Maxwellian thermal distribution, numerical integrations in tabular and graphical form have been given by Harrison, Hummer, and Fite, and in the range $0 \leq \phi \leq 100^o$ or $0 \leq \frac{f\ell}{v} \leq 0.26$, Patterson has obtained by least squares curve fitting the approximation

$$\frac{f\ell}{v} \simeq 2.22 \times 10^{-3}\ \phi + 3.69 \times 10^{-6}\ \phi^2$$

where v is the mean velocity for the Maxwellian distribution:

$$v = \sqrt{\frac{8kT}{\pi m}}$$

Thus if f, $\ell$, and T are known and $\phi$ is measured, the mass of the neutral precursor of any ion is in principle determined.

In practice, $\ell$ is not well known (because the active portion of the ionizer is of non-negligible spatial extent), T is not well known (because of the nature of the source and the free jet expansion), and $\phi$ cannot be measured absolutely because ion flight times and electronic detection and amplification introduce constant, ion mass dependent, and electron energy dependent additional phase shifts. However it is possible to vary $\ell$ by accurately measurable distances, in

which case $\Delta\phi/\Delta\ell$, the phase shift per unit length, can be determined independently of spatial, ion optical, and electronic "end effects". The mathematical details, showing $\Delta\phi/\Delta\ell$ to be very nearly linear in $\sqrt{m}$, are derived in the Appendix.

Figure 4 is a plot of $\Delta\phi/\Delta\ell$ vs. $\sqrt{m}$ measured for ions of m/e = 4, 16, 20, 32, 40 and 48 in a beam containing He, Ne, Ar, $O_3$, and perhaps impurities. The points at m/e 4, 40, and 48 corresponding to He, Ar, and $O_3$, clearly lie on the expected line. Each plotted point is the average of 8 to 10 measurements made at electron energies evenly spaced between about 20 and 100 ev, and as expected these values of $\Delta\phi/\Delta\ell$ are independent of electron energy. Two points are plotted at m/e = 20, one the average of three measurements at electron energies below the threshold for the appearance of $Ar^{++}$, and the other the average of five measurements at electron energies above this threshold. Below the $Ar^{++}$ appearance threshold, $\Delta\phi/\Delta\ell$ clearly corresponds to a neutral precursor of mass 20, i.e. $^{20}Ne$. Above the $Ar^{++}$ threshold, $\Delta\phi/\Delta\ell$ is raised nearly to the value corresponding to $^{40}Ar$. From this example we confirm that above the $Ar^{++}$ threshold the total ion signal at m/e = 20 contains both $^{20}Ne^{+}$ and $^{40}Ar^{++}$ components, $Ar^{++}$ being dominant.

The ions observed at m/e = 16 and 32 both clearly have values of $\Delta\phi/\Delta\ell$ belonging to m/e = 48 rather than 16 or 32, indicating that within the limits of measurement all the ions $O_3^{+}$, $O_2^{+}$, and $O^{+}$ come from $O_3$, i.e., there is no measurable quantity of $O_2$ in the ozone beam. The values of $\Delta\phi/\Delta\ell$ plotted are again the average of 8 to 10 measurements

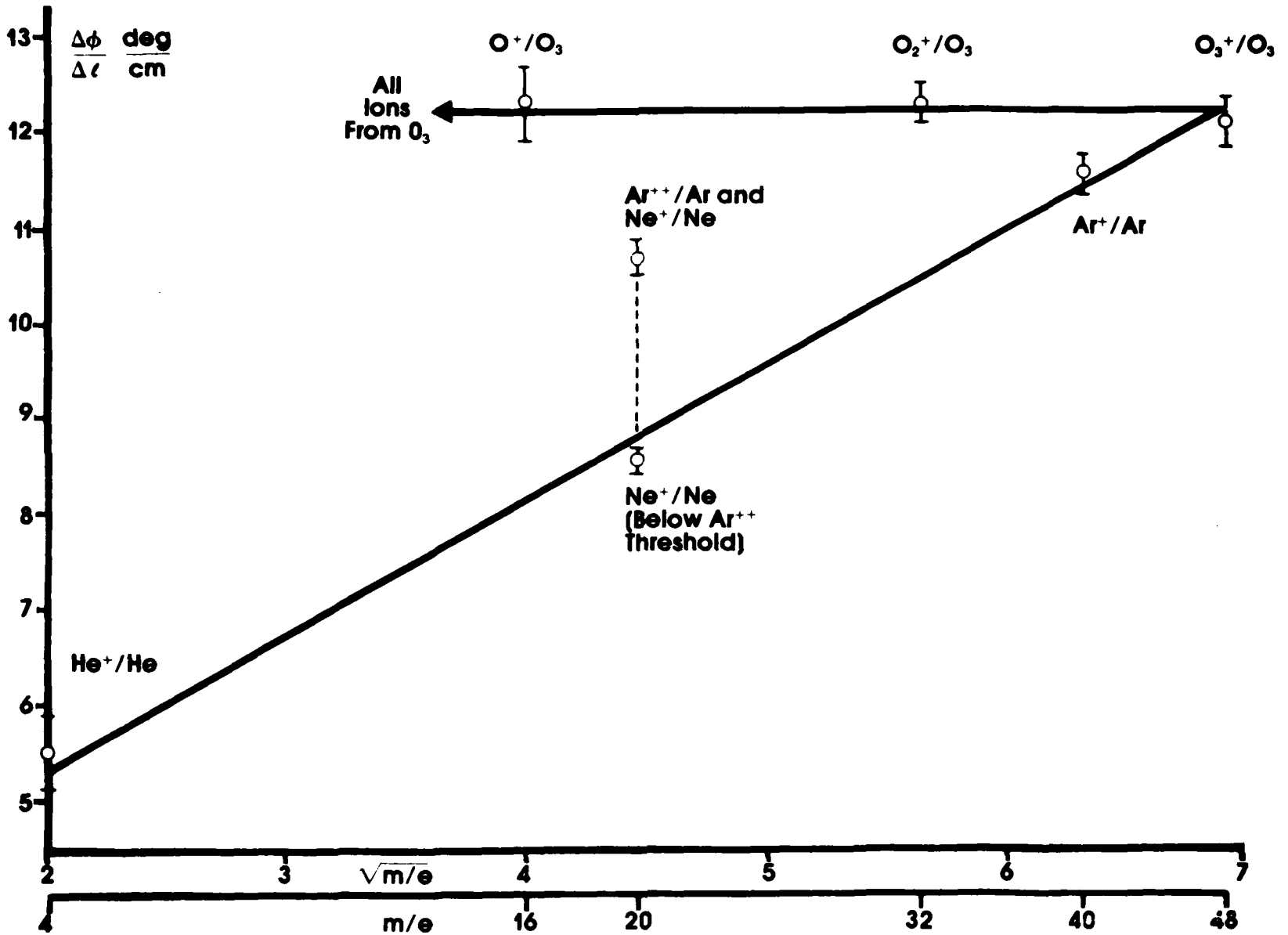


Figure 4
Appendix

evenly spaced in the electron energy range 20-100 ev, and these individual results show no energy dependent trend.

In all cases the absolute phase measurements, $\phi$, are far less reliable than $\Delta\phi/\Delta\ell$. For example, $\phi$ shows a distinct dependence on electron energy, presumably because the electron space charge perturbs the ion energy, while $\Delta\phi/\Delta\ell$ is quite independent of this (or any other) parameter.

Near-Threshold Data

Figures 5 and 6 show composite original data for the appearance of $O_3^+$, $O_2^+$, and $O^+$ from $O_3$, $O_2^+$ and $O^+$ from $O_2$, and $He^+$, $Ne^+$, and $Ar^+$ in the threshold region from approximately 10 to 30 ev. Figure 5 curves are simply superimposed tracings of the raw data. In Figure 6 the data are normalized by pressure, recording sensitivity, and Kieffer's datum for Ar at 28 ev.

The data were obtained in two runs:

1. Ozone source at liquid oxygen temperature, ozone partial pressure $0.5 \times 10^{-1}$ torr, incremental pressure of He, Ne, Ar mixture 0.55 torr, buffer gas composition (atom %) 37% He, 17% Ne, 46% Ar.
2. Ozone source at liquid nitrogen temperature, ozone partial pressure $\approx 10^{-3}$ torr, total pressure 0.6 torr, gas mixture 33% He, 15% Ne, 12% $O_2$, 41% Ar.

The second run was used to generate the $O_2^+$ and $O^+$ from $O_2$ data to determine positively that these threshold curves are different from the $O_2^+$ and $O^+$ from $O_3$ curves.

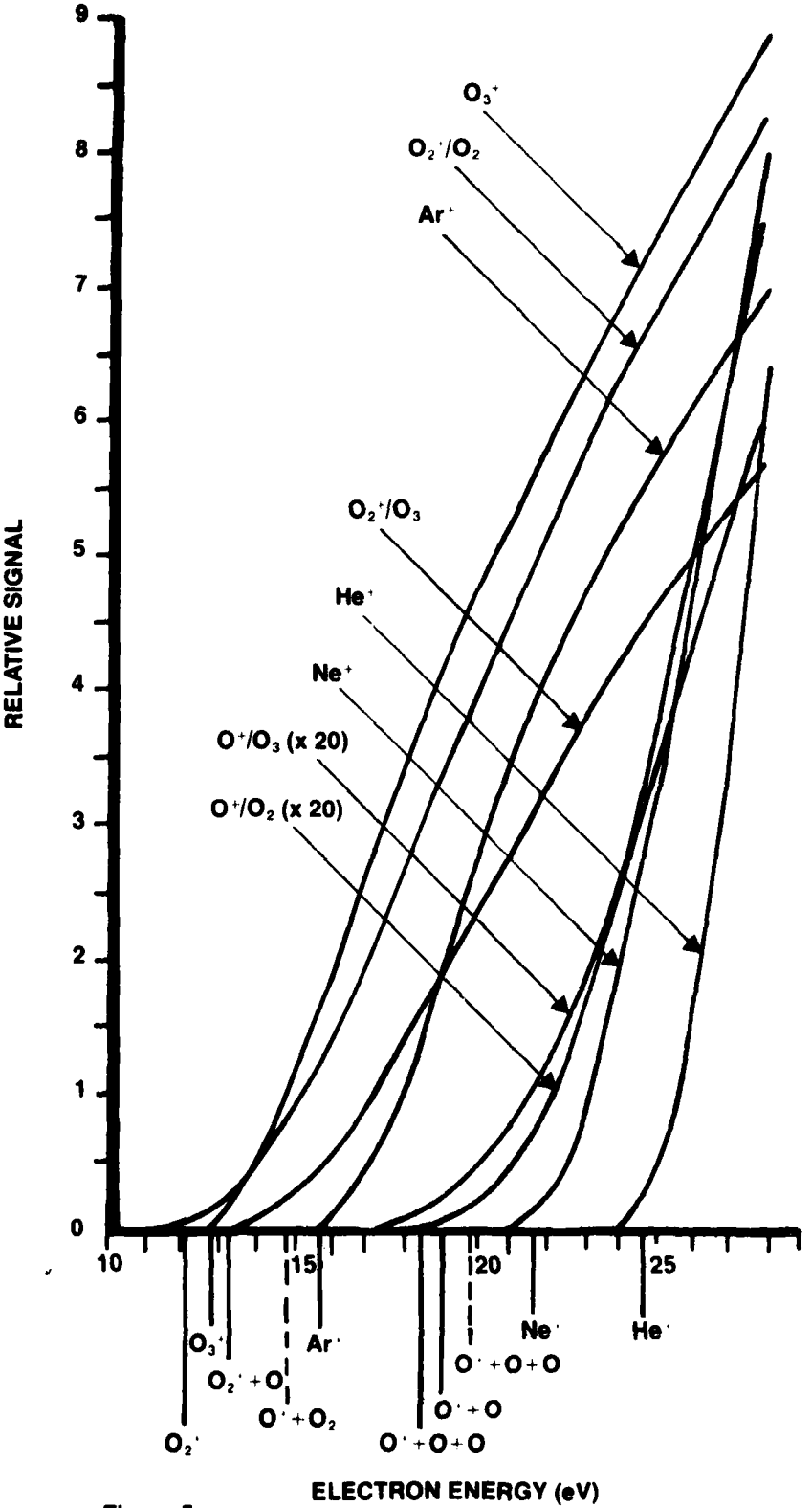


**Figure 5**
**Appendix**

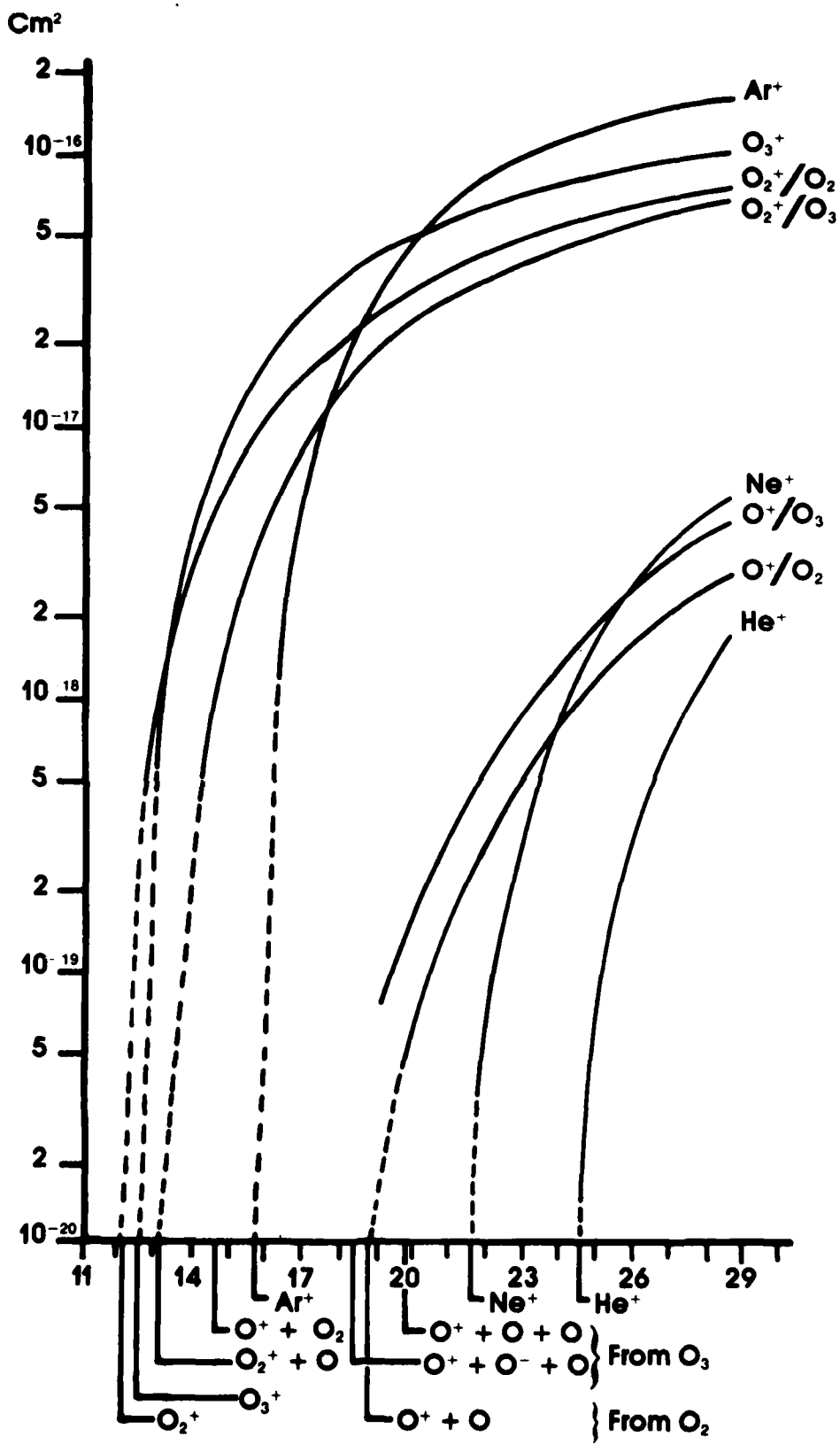


**Figure 6**
**Appendix**

The EMBA-II apparatus is intended to be a high sensitivity analytical instrument, and as such the ionizer is designed to optimize ionization efficiency rather than to provide a well defined electron energy. Thus we are very cautious about claiming the ability to measure absolute ionization potentials with this instrument. Nevertheless the positions of the rare gas and $O_2$ thresholds indicate that ionization potential difference measurements can be made with confidence. To obtain the energy scale for Figures 5 and 6, the nominal electron energy measured at the ionizer control was offset by about 0.6 ev, but the scale factor (ev/mm) was taken directly from the recorder trace. This offset, presumed due to contact potentials, is a reasonable one, and is all that is necessary to bring the rare gas thresholds into good agreement with the known values. The thresholds for production of $O_2^+$ and $O^+$ from $O_2$ are also in good agreement with known values.

Figure 7 shows some energy levels of the three oxygen atom system, indicating known ionization potentials and dissociation energies which are used to predict the appearance potentials of various ionization channels of $O_3$ with ground state products. The channel $O_3 + e \rightarrow O_3^+ + 2e$ has an observed threshold in good agreement with the value known from photoionization (12.67 ev). The channel $O_3 + e \rightarrow O_2^+ + O + 2e$, expected to appear at about 13.14 ev, has a threshold consistent with this value.

But the threshold for appearance of $O^+$ from $O_3$ appears at much too high an electror energy (18-19 ev) to be reasonably assigned to $O_3 + e \rightarrow O^+ + O_2 + 2e$ (14.70 ev), and somewhat too low an energy to

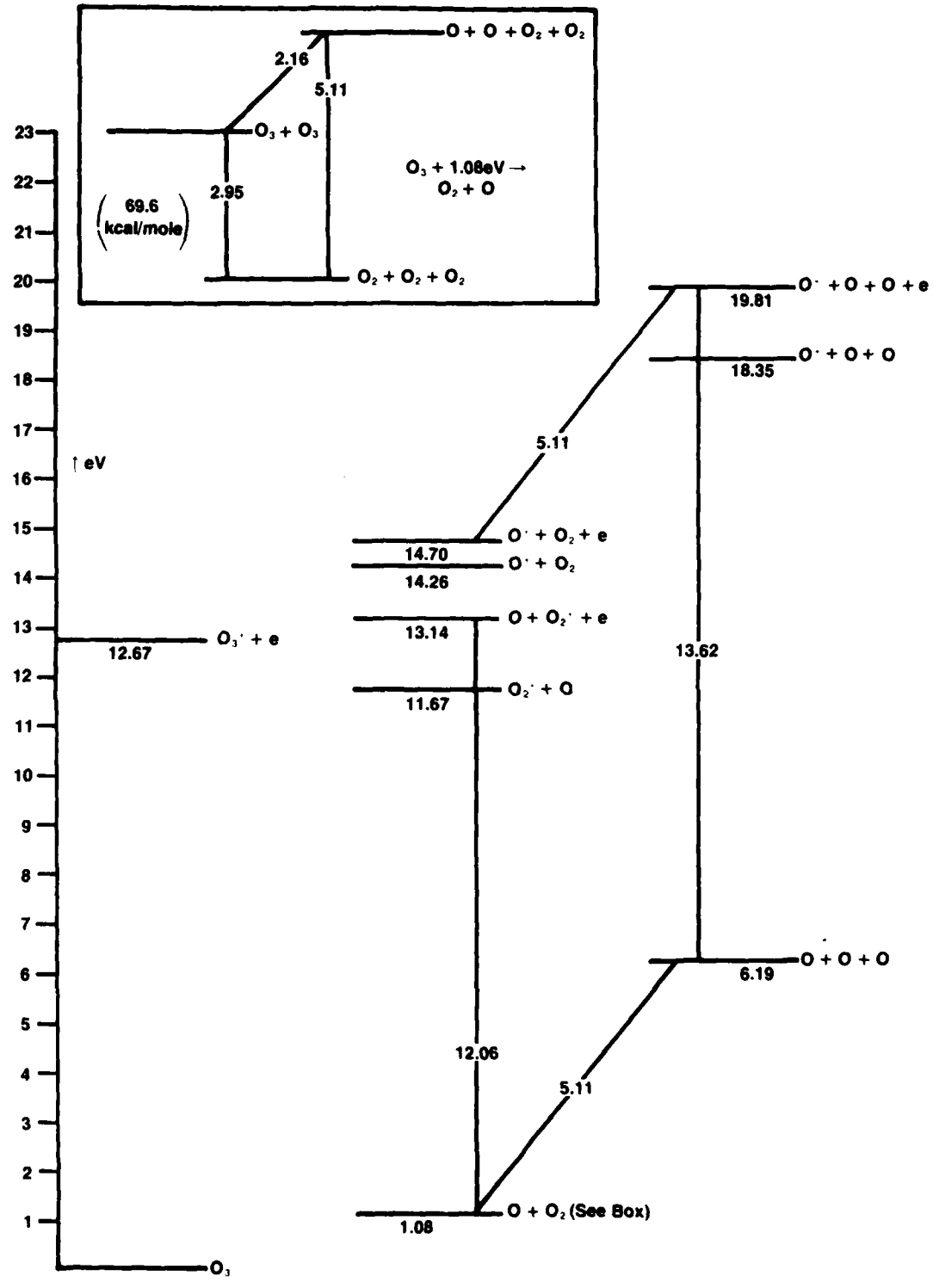


**Figure 7**
**Appendix**

be assigned to $O_3 + e \rightarrow O^+ + O + O + 2e$ (19.81 ev). It is nevertheless clearly distinct from the nearby $O_2 + e \rightarrow O^+ + O + 2e$ curve (18.8 ev), which fact in combination with the phase spectrometry data (Figure 4) makes any confusion with $O^+$ from an $O_2$ impurity unlikely. The channel $O_3 + e \rightarrow O^+ + O + O^- + e$ has a threshold predicted at 18.35 ev, and is the only $O_3$ ionization channel with ground state products whose threshold is close to the observed value. We thus cautiously report that it appears from these results that the dominant channel for production of $O^+$ from $O_3$ may be the doubly dissociative mutual ionization channel

$$O_3 + e \rightarrow O^+ + O + O^- + e$$

We offer no explanation for this, and anticipate checking it at a later time by experiments in which the negative ion is sought.

Broad Range (Threshold to 100 ev) Data

Ion currents of $O_3^+$, $O_2^+$, $O^+$, $Ar^+$, $^{20}Ne^+$, $^{22}Ne^+$, and $He^+$ were recorded logarithmically over a 10-100 ev electron energy range. The logarithmic amplifier was carefully calibrated through the lock-in amplifier's calibration source. The lock-in amplifier output was sufficiently linear and quiet to make this technique useful down to output levels somewhat below $10^{-13}$ of its full scale output. In the absence of instrumental transmission function effects, these ion currents normalized by the respective gas partial pressures in the source and normalized to any one of Kieffer's data points would provide the required absolute cross sections.

In practice, there are at least three sources of systematic error which must be taken into account:

(1) Mass discrimination (fractionation) in the expansion from the nozzle to the ionizer. This is a discrimination depending on the neutral mass.

(2) Mass discrimination in the quadrupole mass filter. This is discrimination depending on the ion mass.

(3) An electron energy dependent sensitivity function due to changes in circulating electron current and space charge depressed potential in the ion production region as the electron energy is changed while holding the emission current constant.

The last of these points is straightforward to handle with confidence, at least in the region above about 30 ev where the cross sections are not varying rapidly with energy. If we normalize our $He^+$ signal to Kieffer's cross section data at one energy (60 ev), and do similarly for Ne and Ar, we can look for systematic deviation as a function of electron energy. We find that our data show a decrease in sensitivity with increasing electron energy. This apparently indicates a decrease in the circulating electron current as the electron energy increases. The magnitude of the effect is shown in Figure 8, which shows the deviation (in mm on a logarithmic plot where 50 mm = 1 decade) between our relative ion currents and Kieffer's relative cross sections for He, Ne, and Ar. (In the case of Ar, the $Ar^{++}$ component has been appropriately accounted for.) If we designate the observed ion current at mass m and electron energy E by $I_o$ (m, E),

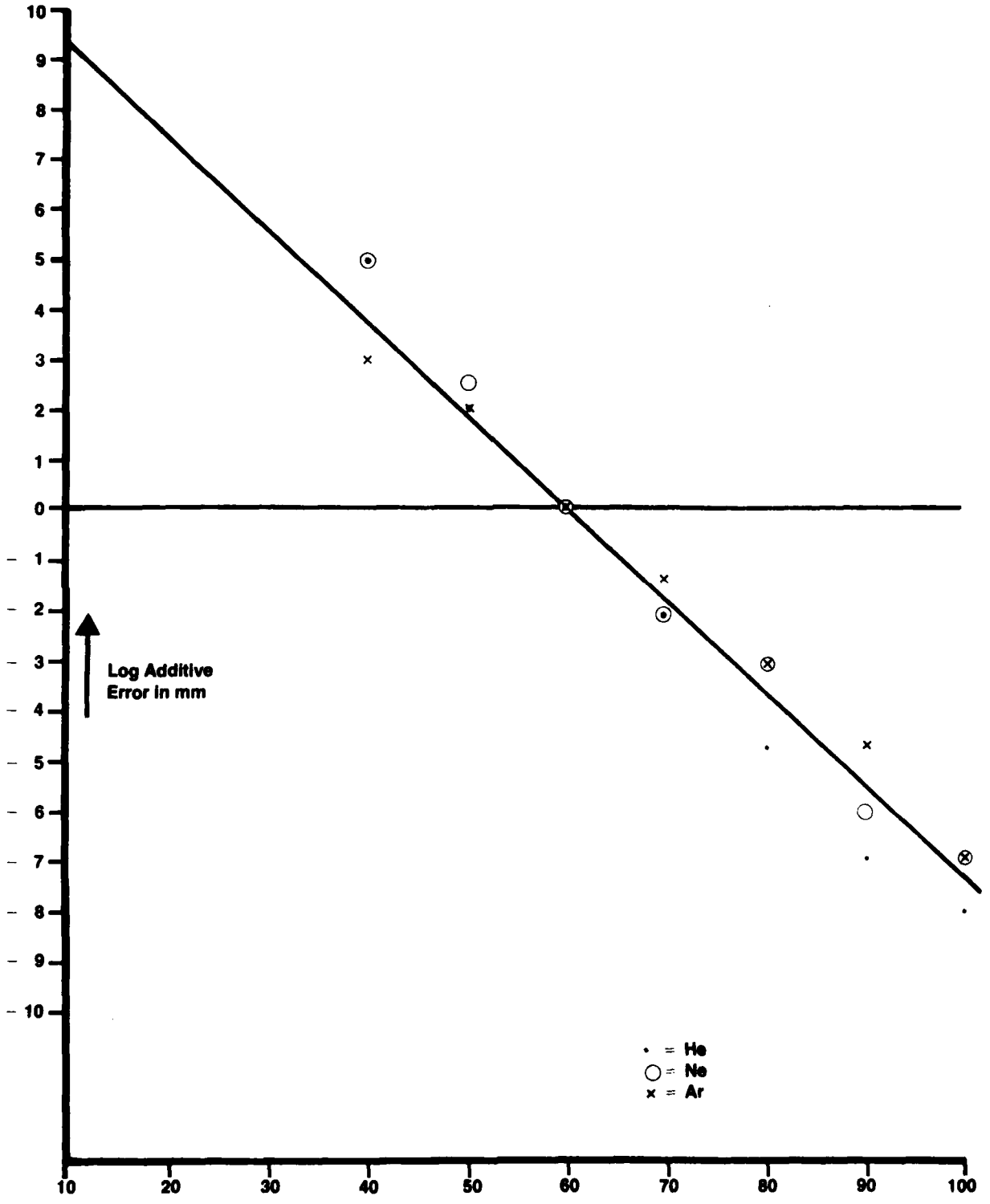


Figure 8
Appendix

then Figure 9 indicates that $I_o$ (m,E) can be corrected for electron energy dependence by letting

$$I_1(m,E) \rightarrow (1.00867)^{(E-60)} I_o(m,E)$$

i.e., the correction is -0.867%/ev. The largest correction generated by this procedure is about 40%.

Mass discrimination is usually attributed entirely to ion mass discrimination, and in the case of quadrupole mass spectrometry is generally blamed (generally vaguely) on the quadrupole. The effect is usually described as a falloff of transmission with increasing mass. In fact, with appropriate electrical adjustment the peak widths can be systematically degraded and the transmission correspondingly enhanced with mass, which at least in part will compensate for an electrical entrance aperture which at fixed peak width inherently becomes smaller with increasing mass. In the mass and resolution range corresponding to these data, the instrument was adjusted to give a transmission slightly increasing with increasing mass.

Mass discrimination in the neutral beam beclouds the issue. If the source operates at a sufficiently low pressure that free molecular flow is applicable, then the number densities of species in the ionizer are all in proportion to their partial pressures in the gas source, i.e., there is no fractionation. On the other hand, if the source operates under viscous flow conditions then all species leave the source with the bulk gas velocity, meaning that the heavy species leave the source relatively more rapidly than under free molecular flow conditions. After expansion and transition to the free molecular flow region the average (in a plane perpendicular to the axis) number

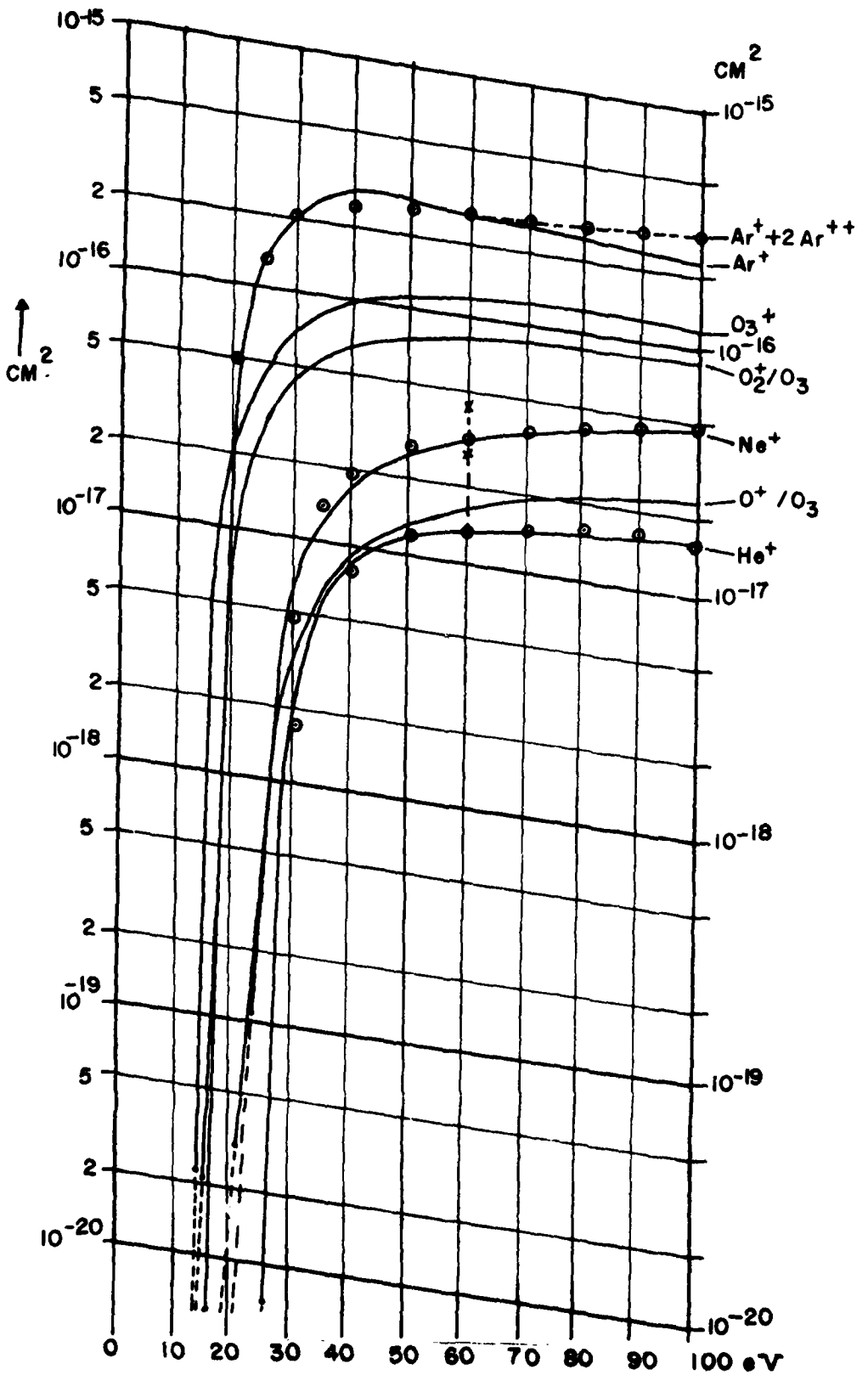


Figure 9
Appendix

density of any species is proportional to the product of its partial pressure in the source and the square root of its mass, so a number density sensitive ionizer will report relatively too high a source partial pressure for heavy molecules. The effect is further enhanced on axis because heavier species are directed into a narrower cone than lighter species. In practice the source operates in the transition region between viscous and free molecular flow, and at most a slight on axis enrichment of heavier species is seen.

The reason neutral mass and ion mass discrimination need to be distinguished is that the former only disturbs our knowledge of the relative partial pressures of He, Ne, Ar, and $O_3$ in the ionizer, while the latter also interferes with our ability to measure accurately the fragmentation pattern of $O_3$ to $O_3^+$, $O_2^+$, and $O^+$.

By comparing our ion currents for $He^+$, $Ne^+$, and $Ar^+$ at 60 ev, normalized by partial pressures, with Kieffer's cross section data, we find (see Figure 9) that we have a relative transmission as a function of mass expressable in this mass range as the straight line

$$I(m) = 0.4 + 0.015m$$

where m denotes ion mass. Since we have experimentally shown fractionation to be small in this apparatus, we assume T(m) is an ion mass discrimination function, and apply it to all observed ion species. Thus observed ion currents are corrected for electron energy sensitivity and ion mass discrimination by the transformation

$$I_2(m,E) = \frac{(1.00867)^{(E-60)}}{0.4 + 0.015m} I_o(m,E)$$

If partial pressures are labelled by a subscript denoting the species molecular weight, M, then our data normalized to Kieffer's datum for Ar at 60ev, $\sigma(40, 60)$ generate normalized absolute cross sections

$$\sigma(m,E) = \frac{(1.00867)^{E-60}}{0.4 + 0.015m} \frac{I_o(m,E)}{I_o(40,60)} \frac{P_{40}}{P_M} \sigma(40,60)$$

These normalized and corrected measurements and Kieffer's data are shown in Figure 10.

**"Figure 10 is unavailable pending final data reduction and evaluation. Tentative values of the information to be included in Figure 10 may be obtained by inspection of Figure 9."**

**Figure 10**

## APPENDIX

The phase shift experienced by a modulated beam of frequency f, flight path $\ell$, and Maxwellian velocity distribution with $v = \sqrt{\frac{8kT}{\pi m}}$ as been shown by least squares fit to the results tabulated in Ref. ( #1) to be numerically approximately by

$$\frac{f\ell}{v} = \alpha\phi + \beta\phi^2 \qquad (1)$$

where $\alpha = 2.22 \times 10^{-3}$ and $\beta = 3.69 \times 10^{-6}$

To second order, the solution of the quadratic equation for small $\frac{f\ell}{v}$ is

$$\phi = \frac{f\ell}{\alpha v}\left(1 - \frac{\beta}{\alpha}\frac{f\ell}{\alpha v}\right) \qquad (2)$$

In practice we measure the change in phase per unit change in $\ell$; in these experiments $\phi$ was measured at the forward position of the quadrupole ($\ell_0$), and at 1 cm intervals ($\ell_0$+1), ($\ell_0$+2),($\ell_0$+3) cm. A least-squares fit attaching equal precision to measured phases at distance increments $\delta$ ($\delta$ = 1 cm here) gives

$$\frac{\Delta\phi}{\Delta\ell} = \frac{1}{10}\left(9\,\frac{\phi(\ell_0+3\delta) - \phi(\ell_0)}{3\delta} + \frac{\phi(\ell_0+2\delta) - \phi(\ell_0+\delta)}{\delta}\right)$$

for the slope. Thus $\Delta\phi/\Delta\ell$ is three times as sensitive to $\phi(\ell_0+3\delta)$ and $\phi(\ell_0)$ as to $\phi(\ell_0+2\delta)$ and $\phi(\ell_0+\delta)$. Since the signal strength, and so the precision of the individual phase measurements, falls off as $\ell^{-2}$, it would be preferable to avoid giving undue weight to the measurement $\phi(\ell_0+3\delta)$. For this reason the data plotted in Figure 3 are actually obtained by the somewhat arbitrary weighting

$$\frac{\Delta\phi}{\Delta\ell} = \frac{\phi(\ell_0+3\delta) - \phi(\ell_0) + \phi(\ell_0+2\delta) - \phi(\ell_0+\delta)}{4\delta} \qquad (3)$$

giving equal weight to all four phase measurements at each electron energy. Substituting (2) into (3) gives

$$\frac{\Delta\phi}{\Delta\ell} = \frac{f}{\alpha v} - \frac{\beta}{\alpha}\left(\frac{f}{\alpha v}\right)^2 \quad (2\ell_o+3\delta)$$

in the specific case of four measurements at $\ell_o$, $\ell_o+\delta$, $\ell_o+2\delta$, $\ell_o+3\delta$. The coefficients of $\ell_o$ and $\delta$, but not the form of the expression, will be different if the number of phase measurements is more than four.

Expressing the velocity in terms of temperature and mass

$$\frac{\Delta\phi}{\Delta\ell} = \left(\frac{f}{\alpha}\sqrt{\frac{\pi}{8kT}}\right)\sqrt{m} - \frac{\beta}{\alpha}\left(\frac{f}{\alpha}\sqrt{\frac{\pi}{8kT}}\right)^2 \quad (2\ell_o+3\delta)m \qquad (4)$$

The term linear in m is small but not entirely negligible compared to the term in $\sqrt{m}$. This means that a plot of $\Delta\phi/\Delta\ell$ vs. $\sqrt{m}$ (i.e., Figure 4) will be approximately linear, but if a fit to a straight line is forced the line will have a positive intercept at zero mass.

Data of the type in Figure 4 are more correctly fit to the quadratic form (4). The least squares fit coefficients of $\sqrt{m}$ and m are given by

$$\frac{f}{\alpha}\sqrt{\frac{\pi}{8kT}} \equiv A = \frac{(\Sigma m_i^{1/2} y_i)(\Sigma m_i^2)(-\Sigma m_i y_i)(\Sigma m_i^{3/2})}{(\Sigma m_i)(\Sigma m_i^2) - (\Sigma m_i^{3/2})^2}$$

and

$$\frac{\beta}{\alpha}\left(\frac{f}{\alpha}\sqrt{\frac{\pi}{8kT}}\right)^2 (2\ell_o+3\delta) \equiv B = \frac{(\Sigma m_i y_i)(\Sigma m_i) - (\Sigma m_i^{1/2} y_i^2)(\Sigma m_i^{3/2})}{(\Sigma m_i)(\Sigma m_i^2) - (\Sigma m_i^{3/2})^2}$$

where $y_i$ is the measured value of $\Delta\phi/\Delta\ell$ at mass $m_i$. For the data in Figure 4, we obtain A = 2.640 and B = 0.1333.

In practical units (m in amu, T in $^{o}$K), and using the required values of $\alpha$ and $\beta$, we have

$$A = 1.815 \times 10^{-3} \sqrt{\frac{293}{T}} \quad f$$

and

$$B = 5.476 \times 10^{-9} \frac{293}{T} f^2 \quad (2\ell_o + 3\delta)$$

In these experiments f was about $1.5 \times 10^{-3}$ sec$^{-1}$ and $\delta$ = 1 cm, from which the measured A = 2.640 confirms that the beam was at about room temperature, as expected. Similarly the measured B = 0.1333 is solved to give $\ell_o$ = 3.9 cm, which is about the expected value of the effective modulator-to-ionizer distance.

## Conclusions*

Phase spectrometry has been shown to be an appropriate means for demonstrating the parity of an ozone beam. Cross sections for the ozone ionization channels leading to $O_3^+$, $O_2^+$, and $O^+$ have been measured in the energy range from threshold to 100 ev. Measurements are relative to literature values for the rare gases Ar, Ne, and He, and the major error source in the graphed and tabulated ozone cross sections are associated with knowledge of the ozone partial pressure in the rare gas buffer mixture. Observed thresholds for $O_3^+$ and $O_2^+$ are as expected, but the observed threshold for $O^+$ suggests interesting effects worthy of further measurements.

*Tentative, pending completion of data analysis.

## Acknowledgements

This work was supported in part by F19628-77-C-0236 and in part by Extranuclear Laboratories, Inc. The author thanks W. L. Fite, R. T. Brackmann, and T. A. Patterson for helpful discussions.

## References

(1) Halsted Harrison, David G. Hummer, and Wade L. Fite, Velocity Dispersion of Square-Modulated Maxwellian Molecular Beams, Boeing Scientific Research Laboratories Flight Sciences Laboratory Technical Memorandum No. 26 (January 1964).

# DNA Distribution List

Department of Defense

Director
Defense Advanced Research Projects Agency
1400 Wilson Boulevard
Arlington, VA 22209

1 cy ATTN: TIO
1 cy ATTN: STO
1 cy ATTN: NRMO

Director
Defense Communications Agency
8th Street and Courthouse Road
Arlington, VA 22204

3 cys ATTN: MEECN Office

Defense Documentation Center
Cameron Station
Alexandria, VA 22314

12 cys ATTN: TC

Director
Defense Nuclear Agency
Washington, D. C. 20305

1 cy ATTN: STTL
1 cy ATTN: DDST
3 cys ATTN: RAAE
1 cy ATTN: RAEV

Department of Defense (Continued)

Joint Chiefs of Staff
Department of Defense
Washington, D. C. 20301

1 cy ATTN: J-6

Director
National Security Agency
Fort George G. Meade, MD 20755

2 cys ATTN: Technical Library

Under Secretary of Defense (Research and Engineering)
Department of Defense
Washington, D. C. 20301

2 cys ATTN: DDS&SS

Department of Commerce

U. S. Department of Commerce
Office of Telecommunications
Institute for Telecommunication Sciences
National Telecommunications and Information Administration
Boulder, CO 80303

2 cys ATTN: W. F. Utlaut

Department of the Army

Commander/Director
Atmospheric Sciences Laboratory
U. S. Army Electronics Command
White Sands Missile Range, NM 88002

1 cy ATTN: DRSEL-BL-SY-S
F. E. Niles

Director
U. S. Army Ballistic Research Laboratories
Aberdeen Proving Grounds, MD 21005

1 cy ATTN: George E. Keller

Commander
U. S. Army Foreign Sciences and Technology Center
220 7th Street, N. E.
Charlottesville, VA 22901

1 cy ATTN: Robert Jones

Department of the Navy

Chief of Naval Operations
Department of the Navy
Washington, D.C. 20350



1 cy ATTN: NOP 985
1 cy ATTN: NOP 094H

Department of the Navy (Continued)

Chief of Naval Research
Department of the Navy
800 North Quincy Street
Arlington, VA 22217

1 cy ATTN: Code 465, R. G. Joiner
1 cy ATTN: Code 427, H. Mullaney

Commander
Naval Electronic Systems Command
Department of the Navy
Washington, D.C. 20360

1 cy ATTN: PME-117
1 cy ATTN: PME-117T
1 cy ATTN: PME-117-21
1 cy ATTN: PME-117-21A
1 cy ATTN: PME-117-22

Director
Naval Ocean Systems Center
Electromagnetic Propagation Division
271 Catalina Boulevard
San Diego, CA 92152

1 cy ATTN: Code 2200, W. F. Moler
1 cy ATTN: Code 2200, Ilan Rothmuller
1 cy ATTN: Code 2200, John Bickel

Director
Naval Research Laboratory
4555 Overlook Avenue, S.W.
Washington, D.C. 20375

1 cy ATTN: Code 7700, Timothy P. Coffey
1 cy ATTN: Code 7709, Wahab Ali
2 cys ATTN: Code 7750, John Davis
1 cy ATTN: Code 2627

Commander
Naval Surface Weapons Center (White Oak)
Silver Spring, MD 20910

1 cy ATTN: Technical Library

Office of Naval Research Branch Office
1030 East Green Street
Pasadena, CA 91106

1 cy

Department of the Air Force

Commander
Air Force Geophysical Laboratory, AFSC
L. G. Hanscom Air Force Base, MA 01731

1 cy ATTN: OPR, James Ulwick
1 cy ATTN: LKB, W. Swider
1 cy ATTN: LKB, K. Champion

Director
Air Force Technical Applications Center
Patrick Air Force Base, FL 32920

1 cy ATTN: TD
1 cy ATTN: HQ 1035th TCHOG/TFS

Department of Defense Contractors

General Electric Company
TEMPO - Center for Advanced Studies
816 State Street
Santa Barbara, CA 93102

1 cy ATTN: Warren S. Knapp
1 cy ATTN: DASIAC

Lockheed Missiles and Space Company
3251 Hanover Street
Palo Alto, CA 94304

1 cy ATTN: J. B. Reagan
1 cy ATTN: W. Imhof
1 cy ATTN: Martin Walt

Mission Research Corporation
735 State Street
Santa Barbara, CA 93101

1 cy ATTN: M. Scheibe
1 cy ATTN: D. Sowle

Pacific-Sierra Research Corporation
1456 Cloverfield Boulevard
Santa Monica, CA 90404

1 cy ATTN: E. C. Field

Pennsylvania State University
Ionospheric Research Laboratory
College of Engineering
318 Electrical Engineering - East Wing
University Park, PA 16802

1 cy ATTN: John S. Nisbet
1 cy ATTN: Les Hale
1 cy ATTN: A. J. Ferraro
1 cy ATTN: H. S. Lee

R&D Associates
4640 Admiralty Way
Marina Del Rey, CA 90291

1 cy ATTN: R. Lelevier
1 cy ATTN: F. Gilmore
1 cy ATTN: R. Turco

The Rand Corporation
1700 Main Street
Santa Monica, CA 90406

1 cy ATTN: Cullen Crain

Professor Chalmers F. Sechrist
155 Electrical Engineering Building
University of Illinois
Urbana, IL 61801

1 cy ATTN: C. Sechrist

Stanford Research Institute
333 Ravenswood Avenue
Menlo Park, CA 94025

1 cy ATTN: Allen M. Peterson
1 cy ATTN: Ray L. Leadabrand

University of Pittsburgh
Dept. of Physics & Astronomy
Pittsburgh, PA. 15260

1 cy ATTN: M.A.Biondi
1 cy ATTN: F.Kaufman
1 cy ATTN: W.Fite

General Electric CO. , Space Division, VFSC
Goddard Blvd., King of Prussia
P.O.Box 8555
Philadelphia, PA 19101

1 cy ATTN: M.H.Bortner
1 cy ATTN: T.Baurer

National Oceanic & Atmospheric Admin.
Environmental Research Laboratories
Dept. of Commerce
Boulder, CO 80302

1 cy ATTN: E.E.Ferguson
1 cy ATTN: F.Fehsenfeld